Journal of Sound and Vibration 330 (2011) 664–684

Contents lists available at ScienceDirect

Journal of Sound and Vibration

journal homepage: www.elsevier.com/locate/jsvi

Seismic wave propagation in laterally inhomogeneous geological region via a new hybrid approach

F. Wuttke [a,*], P. Dineva [b], T. Schanz [c]

[a] Laboratory of Soil Mechanics, Bauhaus-University, 99421 Weimar, Germany
[b] Department of Continuum Mechanics, Institute of Mechanics, Bulgarian Academy of Sciences, 1113 Sofia, Bulgaria
[c] Chair of Foundation Engineering, Soil and Rock Mechanics, Ruhr-University, 44780 Bochum, Germany

ARTICLE INFO

Article history:
Received 15 May 2008
Received in revised form
17 August 2010
Accepted 28 August 2010
Handling Editor: A.V. Metrikine
Available online 24 September 2010

ABSTRACT

2D seismic wave propagation in a local multilayered geological region rested in an inhomogeneous half-space with a seismic source is studied. Plane strain state is suggested. The vertical variation of the soil properties in the half-space is modelled by a set of horizontal flat isotropic, elastic and homogeneous layers. The finite local region is with non-parallel layers and free surface relief. Efficient hybrid wavenumber integration-boundary integral equation method (WNI-BIEM) is proposed, validated and applied for synthesis of seismic signals in the finite soil stratum. The numerical simulation reveals that the developed hybrid method is able to demonstrate the sensitivity of the obtained synthetic signals to the seismic source properties, to the heterogeneous character of the wave path and to the relief peculiarities of the local stratified geological deposit. The advantages and disadvantages of the proposed method are discussed.

1. Introduction

A way to shed light on seismic wave propagation in complex geological profile, consists in developing of high-performance tools to simulate seismic signals. A detailed overview of the approaches developed in the field is given by Sanchez-Sesma [1]. Essentially three main groups of methodologies treat the problem and they are analytical, numerical and hybrid methods. Analytical methods are mainly based on the ray theory, mode matching methods and integral representation theorems. Ray theory [2] and its modifications such as the Maslov asymptotic theory [3], the Kirchhoff–Helmholtz methods [4], Gaussian beams [5], generalized ray method [6] and the Born approximation method [7] are restricted to media with simple geometry. Mode matching techniques are based on the fact that the unknown wave fields are built up by superposition of normal modes of the considered medium. The problem is reduced to the evaluation of a set of coefficients needed for the expansion of the wave field by the normal nodes at a given frequency by satisfy the correct boundary conditions. The modal summation is very useful for synthesizing long-period seismograms. Alternative techniques are the reflectivity method [8] and the generalized R/T coefficient method [9,10] as wavenumber integration method (WNIM) that can compute numerical signals for both long- and short-period signals. A satisfactory agreement between theoretical seismograms obtained by generalized ray method and WNIM is presented in Burdik and Orcutt [11].

The modelling of seismic wave propagation in geological media includes the source, the travel path and the receiving site (see Fig. 1a). It comprises two types of models: (a) all-in-one source–path-site single computational tool demanding an

* Corresponding author.
E-mail addresses: frank.wuttke@uni-weimar.de (F. Wuttke), petia@imbm.bas.bg (P. Dineva), tom.schanz@rub.de (T. Schanz).

0022-460X/$ - see front matter © 2010 Elsevier Ltd. All rights reserved.
doi:10.1016/j.jsv.2010.08.042

Nomenclature

Latin characters

C_{ij}	free term coefficients in BIEs depending on the local geometry
$\mathbf{C}$	vector of unknown constants of the analytical solution of ordinary differential equation for the motion-stress vector
D	damping ratio
$\mathbf{E}$	known structure matrix of the layer in the system for the motion-stress vector
L, h	half-width, depth of a semi-elliptical valley
l_{BE}	length of the boundary element
M_{ij}	seismic moment, with ith arm and jth force direction ($i,j = x,z$)
M_0	seismic scalar moment
M	number of layers in vertically inhomogeneous half-space Ω_0
N	number of layers in laterally inhomogeneous geological region Ω_{LGR}
$\mathbf{p}$	traction vector, $p_j = \sigma_{ij} n_j$, where σ_{ij} and n_j are the components of the stress tensor and the outward normal of the surface element
P_j	components of the seismic unit line source described by the term ΔQ
$\mathbf{P}^*$	traction fundamental solution
$\mathbf{R}$	modified reflection coefficient matrix
$\widehat{\mathbf{R}}$	generalized reflection coefficient matrix (cumulative coefficient)
S	depth (z=S) of the seismic source
t	time variable
$\mathbf{T}$	modified transmission coefficient matrix
$\widehat{\mathbf{T}}$	generalized transmission coefficient matrix (cumulative coefficient)
$\mathbf{u}$	displacement vector
$\ddot{\mathbf{u}}$	acceleration vector
$\mathbf{U}^*$	displacement fundamental solution

Greek characters

α	compressional wave velocity
β	shear wave velocity
δ	dip angle of the fault
ρ	density
ζ	wavenumber
θ	slip or rake angle of the fault
Θ	incident angle of P-wave
λ, μ	lame constants
λ_S	length of the shear wave
Λ	common boundary between Ω_{LRG} and Ω_0
$\mathbf{\Lambda}$	exponential matrix in the system for the motion-stress vector
σ_{ij}	stress tensor
$\mathbf{\Sigma}$	vector of stress components
ϕ	strike angle of the fault
ω	circle frequency

Sub- and Superscripts

(x,z)	position of the observer
$\mathbf{T}^l_{d/u}$	transmission coefficients for plane P- and SV-waves impinging on the lth interface from above and below
$\mathbf{R}^l_{d/u}$	reflection coefficients for plane P- and SV-waves impinging on the lth interface from above and below
$\widehat{\mathbf{T}}^l_{d/u}$	generalized transmission coefficients for plane P- and SV-waves, including multiple reflections, conversions and transmissions on the layers above and below the lth interface
$\widehat{\mathbf{R}}^l_{d/u}$	generalized reflection coefficients for plane P- and SV-waves, including multiple reflections, conversions and transmissions on the layers above and below the lth interface
$\mathbf{\Lambda}^l_{d/u}$	the submatrices representing the upgoing/downgoing waves within the lth layer
$\mathbf{C}^l_{d/u}$	the unknown coefficients of analytical solution of ordinary differential equation for the motion-stress vector inside lth layer, representing the upgoing/downgoing waves within the lth layer
$\mathbf{C}^l_{Pd/Pu}$	the unknown coefficients of analytical solution of ordinary differential equation for the motion-stress vector inside lth layer, representing of upgoing/downgoing P-waves within the lth layer
$\mathbf{C}^l_{Sd/Su}$	the unknown coefficients of analytical solution of ordinary differential equation for the motion-stress vector inside lth layer, representing of upgoing/downgoing SV-waves within the lth layer

Abbreviations and Notations

$\Delta\mathbf{Q}$	stress-discontinuity representing the seismic source
$\Omega_{\mathrm{LGR}} = \bigcup_{i=1}^{N} \Omega_i$	finite local geological region with N non-parallel layers Ω_i
$\Omega_0 = \bigcup_{k=1}^{M} \Gamma_k$	vertically inhomogeneous half-space modelled by a series of M homogeneous flat layers Γ_i, parallel to free surface
BIEM	boundary integral equation method
CPV integral	Cauchy principal value integral
FFT	fast Fourier transformation
MS-BIEM	modal summation-boundary integral equation method
WNIM	wavenumber integration method
WNI-BIEM	wavenumber integration-boundary integral equation method
MSM	modal summation method
MS-FDM	modal summation-finite difference method
FE-BEM	finite element-boundary element method

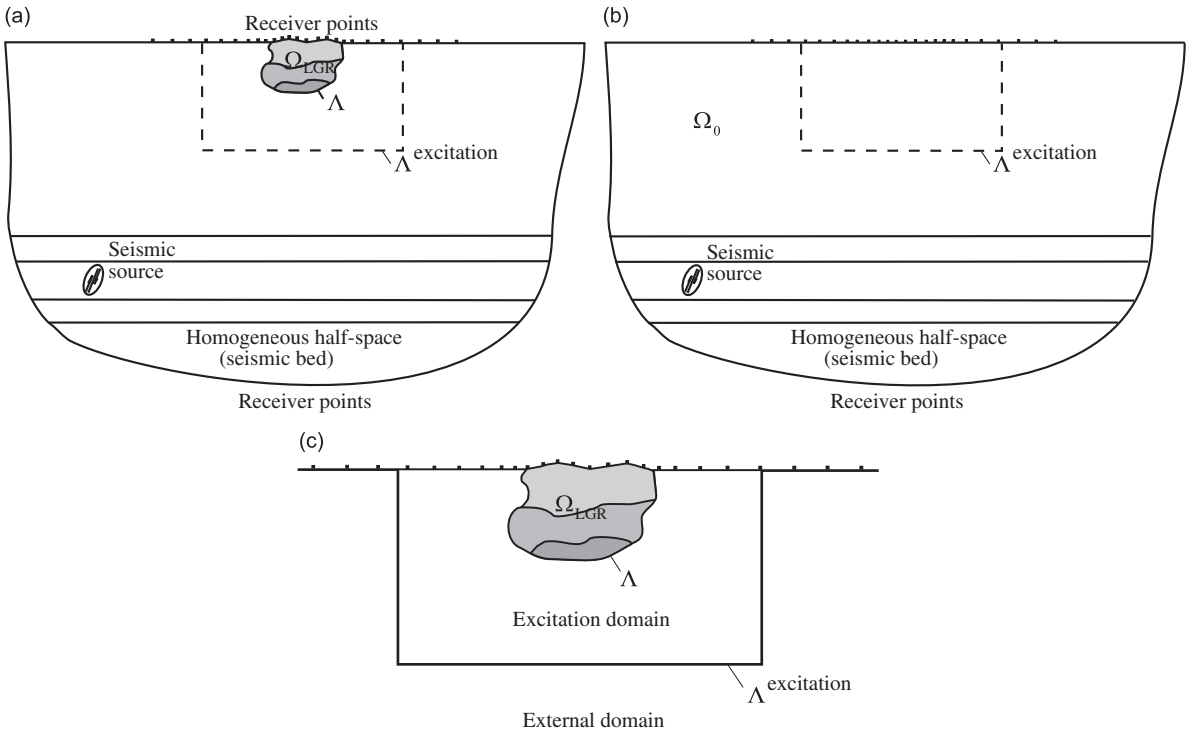

Fig. 1. Scheme of the hybrid WNI-BIEM: (a) original problem configuration; (b) first step: background model and WNIM computation of the free field motion along $\Lambda^{\text{excitation}}$; (c) second step: BIEM computation of the total wave field inside the excitation region and the scattered wave field outside $\Lambda^{\text{excitation}}$.

extreme computer memory and time, especially in the cases the source–receiver distance is measured in dozens of km and (b) hybrid approach based on a two-step procedure that combines the source and path effects (see Fig. 1b) computed by one method and local site effects (see Fig. 1c) evaluated by other method using the first method's wave field as input and basing on the fact that the connection between the two methods keeps the formal wave-injection boundary perfectly permeable for the wave scattered by the local structure. The hybrid methods are especially appropriate when a certain (smaller) part of the model is with more complex topography and geometry than others and it is situated in a large and deep regional model including the source and path effects. The hybrid two-step technique originates by [12] as a domain-coupling technical algorithm. This algorithm was developed and extended further in: (a) [13–16], where the modal summation and finite difference technique is used in the first and second step correspondingly; (b) [17–21] combining the discrete wavenumber method for the regional computation (first step), finite element method for topographic surface parts and finite difference method for localized structures with a flat free surface embedded in a background medium. The same philosophy dates back to works [22,23]. The term "wave injection" was introduced in [24,25]. An efficient seismic modelling requires various methods to be combined, each one being applied just for a single task at which the method performs best. In that way, the individual advantages are enhanced, and the limitations are reduced.

As a whole, the analytical methods are restricted to inhomogeneous media with simple geometry (for example, parallel, horizontal layers in the half-space) and heterogeneity with dimension considerably larger than the prevailing wavelengths and therefore they are only of limited use for zoning studies. This is the reason to use the analytical WNIM to model the wave propagation in inhomogeneous in depth half-space with a seismic source in it. As an analytical tool, the WNIM can give solutions for depths of hundred kilometers without limitations due the CPU time and memory. This is not true for the BIEM, because as a numerical method it has limitations concerning the CPU time and memory. Of course, one of the main advantages of the BIEM is that the fundamental solution used in the construction of the boundary integral equations obeys the radiation condition and thus infinitely extended boundaries are automatically incorporated. In opposite to the BIEM other numerical methods have to use special transmitting, silent and non-reflecting viscous boundaries to satisfy the Sommerfeld's radiation conditions. This very important property is used in the hybrid method essentially as far as the direct BIEM solves both internal and external problems in the second step of the hybrid algorithm. On the boundary between homogeneous and inhomogeneous parts of the half-space, the satisfaction of the Sommerfeld's radiation condition by the WNIM solution has no difficulties. Most of the papers consider analytical approach for solution of the background model and numerical procedure for treating the lateral near-surface soil deposit, see [12–21,25]. Other reasons to use the BIEM to model the wave motion in the local stratified, geological area are the rest of the advantages of this tool: (a) reduce the size of the problem dimensionality and the size of the resulting algebraic system in contrast to other

numerical domain methods; (b) possibility to model lateral inhomogeneity in contrast to WNIM and other analytical approaches; (c) solution at each internal point in the domain is expressed in terms of boundary values without recourse to domain discretization and this main facility is very important when wave propagation problems are being solved in multilayered solids, because only the boundaries between layers are discretized, not their volumes as it is when domain discretization methods as finite element or finite difference methods are used; (d) flexibility to model relief peculiarities in contrast to analytical methods and finite difference method having problems with implementing conditions on boundaries of complex geometric shapes, see [18]; (e) the possibility to obtain directly, with no other intermediate source of error, the dynamic regime — displacements and tractions; (f) the semi-analytical character of the method as far as it is based on Green's function of the considered problem; (g) high level of accuracy is achieved since numerical quadrature techniques are directly applied to the boundary integral equations, which are an exact solution of the considered problem.

Although the advantages of the BIEM are well known, there is still a lack of hybrid methods that are based on this method. Up to now, few BIEM-based hybrid schemes, such as Bard and Bouchon [26,27], Bravo et al. [28], Kawase [29], Bouchon et al. [30], Kawase and Aki [31], Papageorgiou and Kim [32], Zhang et al. [33], Gil-Zepeda et al. [34], Nguyen and Gatmiri [35] have been presented for seismic response analysis of topographic structures. The coupled BIEM with finite element and finite difference methods are proposed in [36–40]. In [41–43], a hybrid approach in which an internal region including the valley under harmonic plane waves is modeled by finite elements, while the exterior region is modeled by the BIE-method. The accuracy and efficiency of the hybrid indirect BIE-Born approximation method is studied in [44]. Gil-Zepeda et al. [34] proposed a hybrid indirect BIEM-discrete wavenumber method and applied it to model the ground motion of stratified alluvial valleys under incident plane SH waves from an elastic homogeneous half-space. An efficient hybrid MS-BIE method based on the modal summation and the direct boundary integral equation technique is developed in [45].

We conclude that there is a lack of hybrid models based on BIEM that allow to take into consideration the properties of all three components: seismic source, inhomogeneous in depth wave path and finite laterally inhomogeneous soil stratum. The majority of the computational tools use the body plane waves as input of the seismic motion in the lateral inhomogeneous geological site. That is not adequate to the real seismic scenarios.

The objective of the present paper is to combine the facilities of both analytical WNI and numerical BIE methods in order to develop an accurate and efficient hybrid approach for synthesis of theoretical seismograms in a laterally varying near-surface seismic region embedded in a deep horizontally layered half-space with a seismic source in one of the layers, accounting for: (a) the seismic source characteristics; (b) the inhomogeneous wave path from the source to the area of interest; (c) the local geological media with the complex mechanical and geometrical properties and (d) the existence of free surface relief peculiarities.

The proposed hybrid technique is based on the WNIM for investigating wave propagation in the background structure, while BIE method is used for synthesis of theoretical seismograms on the free surface of the local finite near-surface soil stratum with or without relief. The hybrid method, as proposed in this paper is most closely resembles to the method discussed in [12–21,25]. The paper has following content: Starting with the problem description in Section 2, followed by the hybrid computational tool presented and discussed in Section 3. The validation study of the computational technique is presented in Section 4. Finally, numerical examples for different seismic scenarios are solved and simulation study is given in Section 5, followed by conclusions in the last Section 6.

2. Problem statement

Consider in-plane seismic wave propagation problem in a near-surface finite local multilayered geological region Ω_{LGR} embedded in a deep first layer of an inhomogeneity in depth, presented by a stack of horizontal layers, which rest on the homogeneous half-space, see Fig. 1a. Plane strain state is suggested. Non-parallel isotropic, elastic and homogeneous layers Ω_i, $i=1,\ldots,N$ are situated in the local soil stratum Ω_{LGR}. The mechanical properties for the inhomogeneity in depth, Ω_0 are modelled with series of M elastic isotropic homogeneous and horizontal layers Γ_i. These layers are parallel to the free surface and overlay the homogeneous half-space — the seismic bed. A seismic source is located in one of the flat layers of the vertical layered part Ω_0 of the half-space. Three types of free surface geometry of the local soil deposit Ω_{LGR} are considered: (a) uniform surface model; (b) canyon model; (c) hill-like model, correspondingly. The objective is to obtain the synthetic seismograms in some receiver points along the free surface of the local near-surface region Ω_{LGR}. The governing wave equations for the lth layer are the following partial differential equations:

$$(\alpha_l^2-\beta_l^2)u_{j,ji}(x,z,t)+\beta_l^2 u_{i,jj}(x,z,t)=\ddot{u}_i(x,z,t) \quad \text{in } Q_B=\Omega_B\, x(0,T) \tag{1}$$

In Eq. (1) commas indicate spatial derivatives, while vectorial quantities are denoted through the use of indices ($i,j=x,z$) and Ω_B comprises the range inside the local geological region and the layered part of the half-space outside it. Longitudinal and shear wave velocities, α_l,β_l, are different for different soil layers in Ω_{LRG}, where $l=1,2,\ldots,N$, and in the layered part of the half-space, where $l=1,2,\ldots,M$, T is the duration of the seismic load, u_i is the displacement, $\ddot{u}_i$ is the acceleration, $i=x,z$. In order to exclude the time variable t and to solve the boundary-value problem in the frequency ω domain a Fourier transform is applied to the time variable. The governing partial differential equation for each lth layer is now of

elliptic type:

$$\left(\frac{(\zeta_s^l)^2}{(\zeta_p^l)^2}-1\right)(u_{z,xz}+u_{x,xx})+u_{x,xx}+u_{x,zz}=-(\zeta_p^l)^2u_x$$

$$\left(\frac{(\zeta_s^l)^2}{(\zeta_p^l)^2}-1\right)(u_{x,xz}+u_{z,zz})+u_{z,xx}+u_{z,zz}=-(\zeta_s^l)^2u_z \tag{2}$$

where $\zeta_p^l=\omega/\alpha_l$ and $\zeta_s^l=\omega/\beta_l$. The boundary-value problem consists of the governing Eq. (2) and the following frequency-dependent boundary conditions, see Fig. 1a: (a) the traction at the free surface is zero; (b) displacement compatibility and traction equilibrium conditions at the boundary between each two layers are satisfied; (c) modeling of the seismic bed by homogeneous half-space with compatibility and equilibrium conditions for displacements and traction at the interface between the homogeneous and inhomogeneous part of the half-space; (d) exclusion of incoming waves into the inhomogeneous part of the half-space out of depth (seismic bed) in the case of absence of a seismic source embedded in homogeneous half-space (Sommerfeld radiation condition). The BVP is solved for a sufficient number of values of frequency and a numerical inverse fast Fourier transformation (FFT) is applied in order to obtain the time-dependent solution. The solution of the boundary-value problem is a vector-value function $u_i(x,z,\omega)$, which complies the Hölder continuity on the boundary $\overline{Q}_B$ and satisfies the system (2) and the boundary conditions given above.

3. Hybrid wavenumber integration — BIE method

3.1. The essence of the hybrid approach

The hybrid WNI-BIEM computation scheme is subdivided into two steps. In the first step, the background 1D-wave field u_i^{fr}, p_i^{fr} in the stack of horizontal, isotropic layers due to a seismic source in one of them is computed. Complete seismograms are stored at the selected locations along an excitation boundary $\Lambda^{\mathrm{excitation}}$, see Fig. 1b. The quantities of u_i^{fr}, p_i^{fr} are named "'*free-field motion*" in [23,34,46], "*background wave*" in [17], "*source radiation and wave propagation in the background 1D medium*" in [47], "*mean wave field obtainable as the response solution for the layered half-space without the lateral inhomogeneity*" in [48,49]. In spite of the used different notations, the mechanical sense is one and the same. It is a wave field corresponding to the 1D medium with no additional local 2D heterogeneity. The 1D model usually represents a stack of flat layers overlaying a half-space, see [47]. This is true in our case, also. Background model solution is the response solution for the horizontally layered half-space *without the lateral inhomogeneity* Ω_{LGR} and *subjected to seismic waves radiate from the seismic source*, see Fig. 1b. It satisfies the elastodynamic wave equation and the following boundary conditions: (a) tractions are zero on the flat free surface; (b) displacement compatibility and traction equilibrium conditions at the boundary between each two flat layers are satisfied; (c) modelling of the seismic bed by homogeneous half-space with displacement compatibility and traction equilibrium conditions at the interface between the homogeneous and inhomogeneous part of the half-space; (d) exclusion of incoming waves into the inhomogeneous part of the half-space out of the depth (seismic bed) in the case of absence of a seismic source embedded in the homogeneous part of the half-space (Sommerfeld radiation condition). The near-surface local geological Ω_{LGR} region is situated entirely inside the excitation domain which is bounded by the excitation boundary $\Lambda^{\mathrm{excitation}}$ and the free surface, see Fig. 1c. In [17–21], the authors named it the excitation box. The seismic source is placed outside the excitation region, see Fig. 1a,b. Inside the excitation region, the medium surrounding the local geological region Ω_{LGR} has the same mechanical properties as in the background field calculation. The free field motion (the background) part is calculated by WNIM, described shortly below. In the second step the seismic source is no longer present and the medium is truncated in a domain comprising the area inside the excitation region and outside the excitation boundary $\Lambda^{\mathrm{excitation}}$ in its close vicinity, see Fig. 1c. The second step modelling comprises detailed local structure with the strongest inhomogeneity and occupies only a fraction of the background model considered in the first step, see [17–21]. The BIEM computes simultaneously the total (complete) wave field u_i^{total}, p_i^{total} in the interior of the excitation region and the scattered u_i^{sc}, p_i^{sc} wave field outside the excitation boundary $\Lambda^{\mathrm{excitation}}$. The quantities of u_i^{sc}, p_i^{sc} are named "*diffracted waves*" in [34–43,46], "*residual field*" in [17,18,23] and "*scattered wave field called also perturbation due to the lateral inhomogeneity*" in [48,49]. In spite of the used different notations, the mechanical sense is one and the same and it is the scattered by the local inhomogeneity wave. The scattered wave field is defined by the difference $u_i^{\mathrm{sc}}=u_i^{\mathrm{total}}-u_i^{\mathrm{fr}}$, $p_i^{\mathrm{sc}}=p_i^{\mathrm{total}}-p_i^{\mathrm{fr}}$. The complete wave field inside the excitation region (internal problem) and the scattered wave field outside the excitation boundary (external problem) are computed by the BIEM simultaneously. These fields are coupled by means of the boundary conditions relating u_i^{total}, p_i^{total} on the inner side of the excitation boundary with scattered wave u_i^{sc}, p_i^{sc} on the outer side of the boundary, satisfying the welded contact. The saved and recorded background wave field in the first step u_i^{fr}, p_i^{fr} is used as "implemented" boundary conditions on the excitation boundary to generate the wave field as if it enters the excitation region outside. The truncation of the background model is an approximation that neglects interaction of the scattered wave with cropped parts of the 1D model (stack of horizontal, isotropic layers) as deeper layers. The obtained solution does not contain information about the interactions between the residual wave field and the structural features deeper than the BIEM domain, see [17–21]. The excitation domain is chosen to encompass the local structure of interest. The outside of the excitation domain with further interfaces and inhomogeneities is truncated and only the necessary volume defined after validation study is left.

So, the truncation limits the interactions between the structure of interest and the outer medium to the interaction with contents of the incoming background wave field, i.e. it may include surface and body waves influenced by the source, wave path and the structure around (in close vicinity of) the excitation domain. The multiple reflections of the scattered wave between the local structure of interest inside the excitation domain and the regional structure outside it can be modelled properly by the optimal choice of the truncated domain based on the validation study.

3.2. WNIM–BIEM coupling

The key point of the hybrid method is the presentation of the total wave field by a sum of the free field (background) and the scattered parts: $u_i^{\text{total}}=u_i^{\text{fr}}+u_i^{\text{sc}}$, $p_i^{\text{total}}=p_i^{\text{fr}}+p_i^{\text{sc}}$. The total wave field is inside the excitation domain, while the scattered wave field is propagating outside of the excitation domain. The boundary conditions relating the total wave field on the inner side of the excitation boundary with scattered wave *on the outer side of the boundary*, *satisfying the welded contact*. The hybrid coupling keeps the excitation boundary fully transparent in the second step. The scattered wave field penetrates freely out of the excitation domain and, if reflected by an inhomogeneity, it freely propagates through the excitation boundary back into the local structure. Oprsal et al. [19] discussed clearly the essence of the generalized hybrid approach of wave injection based on binding two sub-volumes treated by arbitrary wave propagation methods. The decomposition of the total wave field into a sum of free field motion and the scattered wave is commented in the same manner in [60] for the case of the seismic response of a foundation rested in a non-homogeneous half-space.

3.3. WNIM solution for free field wave motion u_i^{fr},p_i^{fr}

In the first step, the seismic source radiation and wave propagation in the horizontally layered background medium Ω_0 is calculated by the WNIM, and the computed background wave field $\mathbf{U}^{\mathbf{fr}}$ (called free-field) is recorded along the excitation boundary $\Lambda^{\text{excitation}}$, see Fig. 1b. The WNIM solves the problem for wave propagation in horizontally layered media with a seismic source at a given level $z=S$ and rested on homogeneous half-space, where radiation condition is satisfied. The unknowns are displacements $u_i^{l,\text{fr}}(x,z,t)$ and traction $p_i^{l,\text{fr}}(x,z,t)=\sigma_{ij}^{l,\text{fr}}n_j$ in each lth layer, where $i=x,z$. The basic equations (1) are decoupled by application of the Helmholtz decomposition theorem into potentials, see [8]. Since the elastic properties do not depend on horizontal position, we use the Fourier transforms over time and the horizontal coordinate to reduce the partial differential equations of motion to a set of ordinary differential equations according to the displacement $\mathbf{u}^{l,\text{fr}}(\zeta,z,\omega,S)$ and stress $\mathbf{\Sigma}^{l,\text{fr}}(\zeta,z,\omega,S)$ vectors which depend on the frequency ω , wavenumber ζ, location of the observer z and source depth S. After applying the inverse Fourier transformation to the wavenumber ζ, unknown displacement and stresses are obtained in the frequency-space domain. The frequency-domain formulation is based on the representation of the complete response in terms of semi-infinite integrals with respect to the wavenumber. The integrands for each wavenumber and frequency are determined by an efficient factorization in terms of generalized transmission and reflection coefficients which are calculated by an iterative scheme. As far as we consider the case, when the lateral inhomogeneous soil deposit is situated in the first layer of the horizontally layered half-space (see Fig. 1a) we need the WNIM solutions for displacement $\mathbf{u}^{l,\text{fr}}(x,z,\omega)$ and stress $\mathbf{\Sigma}^{l,\text{fr}}(x,z,\omega)$ vectors in the first layer $l=1$. Following notation and mathematical description in [9,10,52,54,55,70], these analytical expressions are given as follows:

$$\mathbf{u}^{1,\text{fr}}(x,z,\omega,S)=\frac{1}{2\pi}\int_{-\infty}^{\infty}(\mathbf{E}_{11}^1\mathbf{\Lambda}_d^1\widehat{\mathbf{R}}_u^0+\mathbf{E}_{12}^1\mathbf{\Lambda}_u^1)\widehat{\mathbf{T}}_u^1\widehat{\mathbf{T}}_u^2\ldots\widehat{\mathbf{T}}_u^{S-1}(\mathbf{B}^{S+}\mathbf{D}^S-\mathbf{B}^{S-})^{-1}\Delta\mathbf{Q}\,\mathrm{e}^{(\mathrm{i}\zeta x)}\,\mathrm{d}\zeta \tag{3}$$

$$\mathbf{\Sigma}^{1,\text{fr}}(x,z,\omega,S)=\frac{1}{2\pi}\int_{-\infty}^{\infty}(\mathbf{E}_{21}^1\mathbf{\Lambda}_d^1\widehat{\mathbf{R}}_u^0+\mathbf{E}_{22}^1\mathbf{\Lambda}_u^1)\widehat{\mathbf{T}}_u^1\widehat{\mathbf{T}}_u^2\ldots\widehat{\mathbf{T}}_u^{S-1}(\mathbf{B}^{S+}\mathbf{D}^S-\mathbf{B}^{S-})^{-1}\Delta\mathbf{Q}\,\mathrm{e}^{(\mathrm{i}\zeta x)}\,\mathrm{d}\zeta \tag{4}$$

The integrands in Eqs. (3) and (4) are functions of wavenumber ζ and depend on the characteristics of the soil stratum, frequency, the depth of the seismic source and the location of the observer. In the above equations the generalized reflection/transmission (R/T) coefficients are denoted by $\widehat{\mathbf{R}}_u^l=\mathbf{R}_u^l+\mathbf{T}_d^l\widehat{\mathbf{R}}_u^{l-1}\widehat{\mathbf{T}}_u^l$ and $\widehat{\mathbf{T}}_u^l=(\mathbf{I}-\mathbf{R}_d^l\widehat{\mathbf{R}}_u^{l-1})^{-1}\mathbf{T}_u^l$, $l=1,\ldots,S-1$ for the layers above the source and $\widehat{\mathbf{R}}_d^l=\mathbf{R}_d^l+\mathbf{T}_u^l\widehat{\mathbf{R}}_d^{l+1}\widehat{\mathbf{T}}_d^l$ and $\widehat{\mathbf{T}}_d^l=(\mathbf{I}-\mathbf{R}_u^l\widehat{\mathbf{R}}_d^{l+1})^{-1}\mathbf{T}_d^l$, $l=M-1,\ldots,S$ for the layers below the source. For $l=M$ the generalized reflection coefficients are $\widehat{\mathbf{R}}_d^l=\mathbf{R}_d^M$ and $\widehat{\mathbf{T}}_d^M=\mathbf{T}_d^M$, where $\mathbf{R}_d^M$ and $\mathbf{T}_d^M$ are the modified R/T coefficients for the layer M. The index l of layers is running from 1 to M, and the seismic bed is homogeneous half-space and denoted by $M+1$. The term $\widehat{\mathbf{R}}_u^{l-1}=\widehat{\mathbf{R}}_u^0$ is the reflection coefficient at the free surface as the upper boundary of the first layer. The seismic line source in vertical or horizontal direction is described by the term $\Delta\mathbf{Q}=[-P_x,0]^T$ and $\Delta\mathbf{Q}=[0,-P_z]^T$, where P_x and P_z are unit line loads in horizontal and vertical directions. Matrix $\mathbf{I}$ describes the unit matrix, while the power of -1 means the inverse of a matrix. The matrices $\mathbf{E}$ contain the variables excluding exponents and amplitudes of the analytical solution for each layer. The matrix expressions for displacements and stresses are as follows:

$$\mathbf{u}^{l,\text{fr}}(\zeta,z,\omega)=\mathbf{E}_{11}^l\mathbf{\Lambda}_d^l\mathbf{C}_d^l+\mathbf{E}_{12}^l\mathbf{\Lambda}_u^l\mathbf{C}_u^l \tag{5}$$

$$\mathbf{\Sigma}^{l,\text{fr}}(\zeta,z,\omega)=\mathbf{E}_{21}^l\mathbf{\Lambda}_d^l\mathbf{C}_d^l+\mathbf{E}_{22}^l\mathbf{\Lambda}_u^l\mathbf{C}_u^l \tag{6}$$

where the terms $\mathbf{\Lambda}^l_{d/u}$ describe the wave propagation in positive (down) and negative (up) directions in the lth layer. The submatrices $\mathbf{\Lambda}^l_{d/u}$ and $\mathbf{E}^l_{ij}$, i=1,2, j=1,2, are functions of shear modulus μ^l, shear β^l and compressional α^l wave velocities, wavenumber ζ, frequency ω and $z \in (z^{l-1},z^l)$. The terms $\mathbf{C}^l_{Pd/Pu}$ and $\mathbf{C}^l_{Sd/Su}$ are the unknown constants of the solution of the ordinary differential equation, in the lth layer that describe up and down going P- and SV-wave propagation, see [9,53]. The quality factor or its inverse the dissipation factor describing the material attenuation in soil is defined by the material damping ratio that in the numerical studies here is assumed to be depth dependent. For layers embedded in a depth smaller than 1 km the material damping ratio is 1%, in a depth between 1 and 5 km the material damping ratio is 0.5% and for layers in a depth more than 5 km the damping ratio is 0.25%. By following the definition of the complex velocities [9], the singular points of the integrals in Eqs. (5) and (6) are shifted slightly from the wavenumber real axis in the complex plane. The numerical integration along the real wavenumber axis can be done without singularities. Finally, the displacement function in the frequency and space domain is obtained after integration over all wavenumbers along the integration path. The displacements in the time and space domain are obtained by inverse Fourier transformation procedure.

3.4. BIEM solution in the second step

In this second step, the BIEM computes simultaneously the total (complete) wave field in the interior of the excitation region and the scattered wave field outside the excitation boundary. The following system of boundary integral equations according to the total wave field is satisfied along the boundaries of the layers inside the excitation region:

$$C_{ij}u_i(x,z,\omega) = \int_{\Omega_m} U^*_{ij}(x,z,x_0,z_0,\omega)p_j(x_0,z_0,\omega)\,\mathrm{d}\Gamma - \int_{\Omega_m} P^*_{ij}(x,z,x_0,z_0,\omega)u_j(x_0,z_0,\omega)\,\mathrm{d}\Gamma \tag{7}$$

m=1,2,3,…,N here, and C_{ij} are the constants depending on the geometry at the collocation point (x,z); (x_0,z_0) denotes the position vector of the source point; Γ_{Ω_m} is the boundary of the Ω_m layer; u_i and p_j are the unknown total displacements and tractions on the boundaries Γ_{Ω_m}; U^*_{ij}, P^*_{ij} are the displacement and traction frequency-dependent fundamental solutions of Eq. (2), given in [50]. The BIE on the external boundary $\Lambda^{\text{external}}$ is added and it is according to the scattered wave field, which in this case is $u_i^{\text{sc}}=u_i^{\text{total}}-u_i^{\text{fr}}$, $p_i^{\text{sc}}=p_i^{\text{total}}-p_i^{\text{fr}}$.

$$\begin{aligned} C_{ij}(u_j^{\text{total}}(x,z)-u_j^{\text{fr}}(x,z))|_{\Lambda^{\text{external}}} = &\int_{\Lambda^{\text{external}}} U^*_{ij}(x,z,x_0,z_0,\omega)(p_j^{\text{total}}(x_0,z_0)-p_j^{\text{fr}}(x_0,z_0))\,\mathrm{d}\Gamma \\ &-\int_{\Lambda^{\text{external}}} P^*_{ij}(x,z,x_0,z_0,\omega)(u_j^{\text{total}}(x_0,z_0)-u_j^{\text{fr}}(x_0,z_0))\,\mathrm{d}\Gamma \end{aligned} \tag{8}$$

The system of BIE (7) and (8) is according to the unknown displacement u_i^{total} and traction p_i^{total} on the boundaries of the layers in the local geological structure, on the boundary of the excitation region and on the observer points on the free boundary. In order to solve this system of BIEs we need to know the free field motion u_i^{fr}, p_i^{fr} at the boundary nodes on the external boundary $\Lambda^{\text{external}}$. The values for u_i^{fr}, p_i^{fr} in the boundary nodes on $\Lambda^{\text{external}}$ are obtained as solution of the background problem by WNIM. The usual numerical procedure of BIEM is applied. The boundary is discretized into elements using piecewise polynomial approximations of the boundary geometry, displacement and traction. The mesh discretization is made via the quadratic boundary element method. After discretization, in the Fourier transformed domain the kernels of the obtained integrals have singularities like (a) $O(1/c\pm\xi)$, for $c\in[-1;+1]$ that lead to the *Cauchy principal value* (CPV) integrals and (b) singularities like $O(\ln(c\pm\xi))$ for $c\in[-1;+1]$ that lead to non-singular integrals. The regular integrals are computed employing the Gaussian 32-point quadrature scheme and boundary element subdivision, while the singular integrals are solved analytically, using the asymptotics of the fundamental solutions for small arguments, see [51]. After application of discretization procedure, the system of boundary integral equations is transformed into an algebraic system for the unknown displacement and traction in the Fourier domain. To obtain displacements and tractions as functions of time, the inverse Fourier transformation is applied.

4. Validation study

The aim of the validation study is to establish the error bounds of the proposed hybrid tool and to evaluate its accuracy on the base of solution of several benchmark examples. The validation of the proposed hybrid solution is based on the comparison to pure analytical or numerical methods or other hybrid computational techniques. The first example validates the proposed hybrid WNI-BIEM technique by solution of specially selected benchmark example which can be solved by the pure analytical methods and by the proposed hybrid method. The second and the third numerical examples validate the accuracy of the BIEM that is one of the base components of the proposed hybrid technique.

The fourth test example concerns comparison of the numerical results obtained by the proposed WNI-BIEM with two other hybrid techniques as modal summation-BIEM (MS-BIEM) and modal summation-finite difference method (MS-FDM).

Test example 1. As a first test example a structural model given in Fig. 2a is used.

The local geological region Ω_{LGR} in Fig. 2a is a valley $L_1R_1T_1P_1$ and it is situated in the first layer of a layered half-space. The coordinates of the corner points (in meters) are: $T_1(100,0)$, $P_1(-100,0)$, $L_1(110,270)$, $R_1(-110,270)$. The mechanical properties of the local geological region are the same as the first layer in the horizontally layered half-space. In this case it

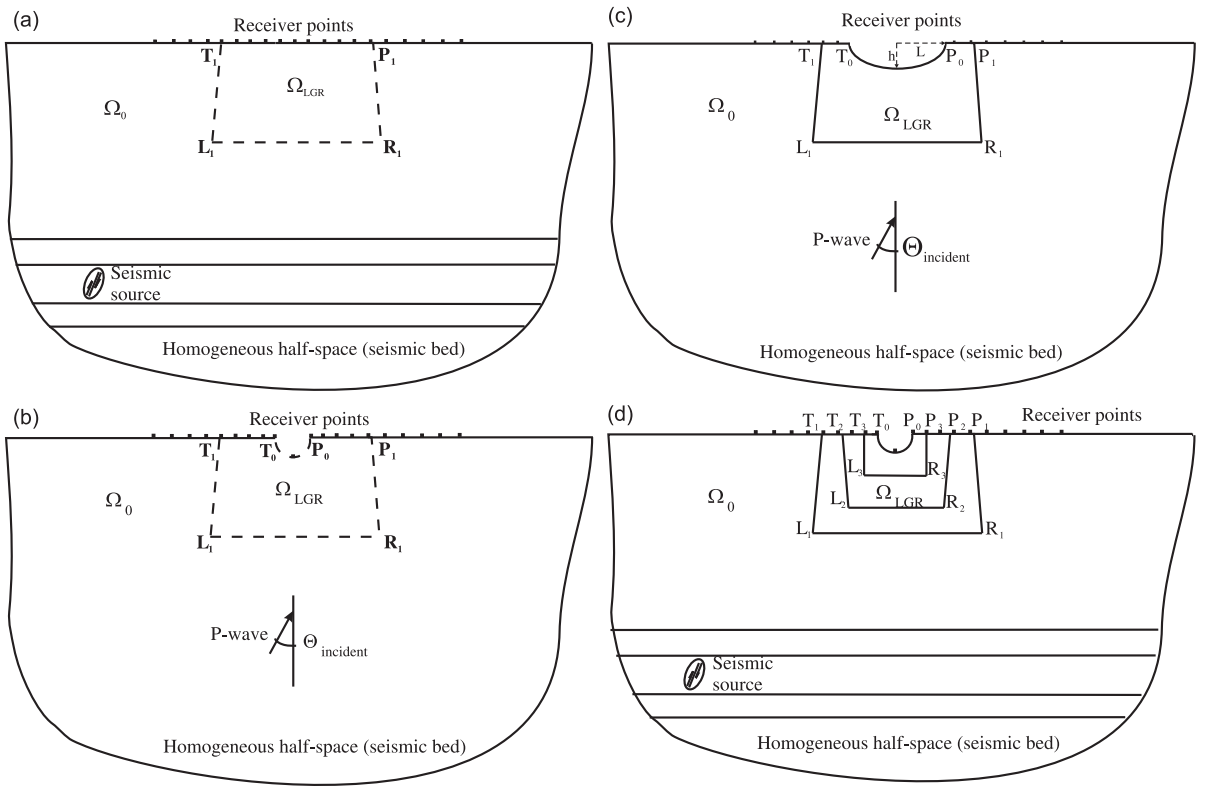

Fig. 2. The geometry of the numerical examples: (a) test example 1; (b) test example 2; (c) test example 3; (d) test example 4.

is possible to solve the problem by both methods—by the pure WNIM and by the proposed hybrid WNI-BIEM. The comparison between studied hybrid solutions against pure WNIM results can evaluate and place the accuracy bounds of the developed hybrid computational technique. The same validation philosophy can be seen in [14], where the proposed hybrid modal summation-finite difference method (MS-FDM) is verified by solution of the background 1D model (background model is the same as in our case: horizontal flat layers with a seismic source in one of them) by both the pure analytical modal summation method (MSM) and the hybrid MS-FDM. The density ρ_i, the longitudinal wave velocity α_i, the shear wave velocity β_i and the depth of the layers presenting a non-homogeneous in depth half-space are given in Table 1. Two wave paths (1 and 2) are considered with different mechanical properties. A buried vertical line source is defined in wave path 1 at $x=2$ km and at a depth of 2 km and in wave path 2 at $x=2$ km and at a depth of 6 km. Figs. 3a–h show that frequency-dependent displacement components at receiver point (0, 0), obtained by the WNIM and by the hybrid computational tool, are almost identical for both wave paths. The hybrid numerical scheme perfectly replicates the background wave field and this fact demonstrates that the proposed hybrid method works accurately. It is necessary to execute the validation study for each new seismic scenario, because the comparison between the pure analytical method and the proposed hybrid method allows establishing control over the accuracy of the BIEM part of calculations that depends on the correct mesh discretization. The accuracy condition in the BIEM discretization procedure requires that $(\lambda_S/l_{BE}) \geq 10$, where l_{BE} is the length of the boundary element, λ_S is the shear wavelength. So, special attention is needed at high frequencies and for very soft soil layers, where the wave length is small. It is clear that to reach high-numerical accuracy in these cases a very fine BEM mesh is necessary.

Test example 2. The elastic half-plane with surface topography subjected to incident longitudinal time-harmonic P-wave.

In this test example, the pure BIEM is used to compute the free surface displacement components in a homogeneous half-plane with surface topography in the form of circular cylindrical canyon subjected to incident longitudinal P-wave. This problem was solved analytically in [56] for cylindrical canyons with variable width-to-depth ratios. In particular, we focus on the case where this ratio is equal to 1.0, the incident wave angle is 60°, Poisson's ratio for the homogeneous half-plane is 0.25, longitudinal wave velocity is of 5277 m/s, the value of the dimensionless parameter $\eta = 2A/\lambda_s$ is 0.25, where $r=A$ is the canyon radius. Fig. 2b shows the geometry of this analyzed example. The local geological region is the trapezoidal value $T_1P_1L_1R_1$ that is as those in the test example 1, but on the free surface there is a semi-circular canyon and the prescribed material properties are the same as in the homogeneous half-space, considered in this case. This example evaluates the convergence of the BIEM solution by comparison of the authors' results with the analytical solution in [56]. The necessary accuracy was reached at discretization mesh of 64 boundary elements of quadratic type and Figs. 4a and b show comparison of the surface displacement

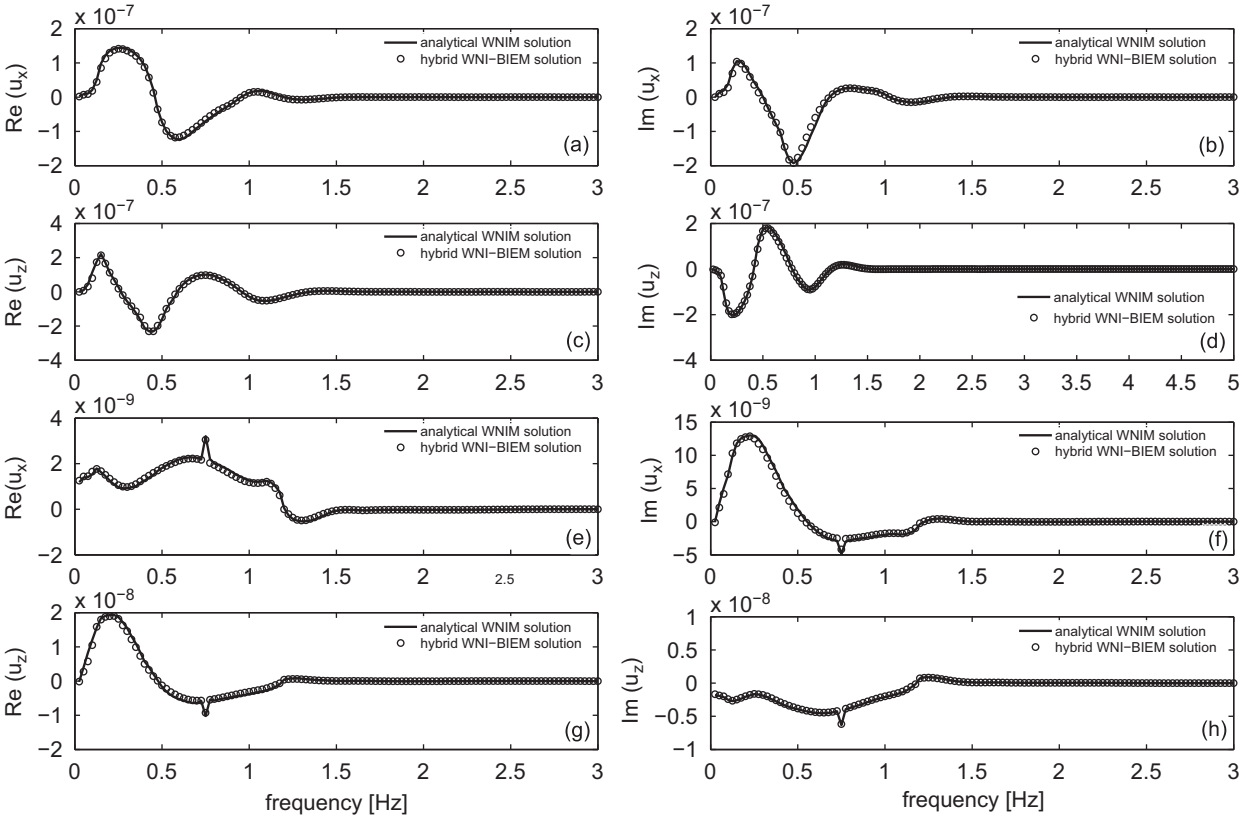

Fig. 3. Real and imaginary part of displacement components vs frequency at receiver point (0, 0): (a)–(d) for wave path 2; (e)–(h) for wave path 1.

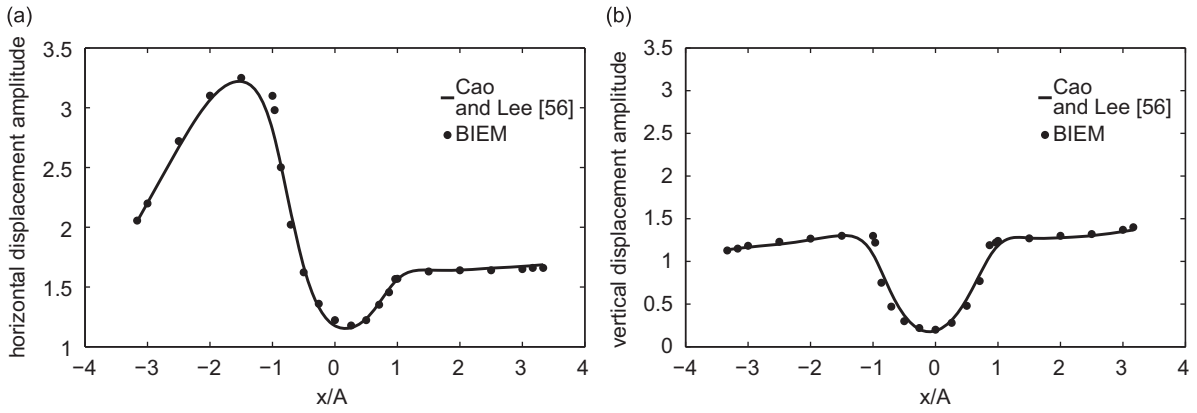

Fig. 4. Surface displacement amplitudes vs x/A on the free surface of homogeneous half-space with a circular canyon of radius $r=A$ under incident longitudinal P-wave: (a) horizontal component; (b) vertical component.

components obtained by BIEM and in [56] vs value of x/A. The both results are very close and this shows that the BIEM works accurately and the chosen discretization mesh gives the convergence results. The similar validation strategy aiming to evaluate the accuracy of other hybrid technique, the hybrid finite element-boundary element method (FE-BEM), was solved in [39], where the diffraction of a plane SV wave of vertical incidence by a semi-circular canyon in an elastic half-space is considered. However, according to the authors, the validation study of the proposed here hybrid WNI-BIEM should be completed by considering more complex benchmark example for a finite soil stratum with non-parallel interfaces situated in an inhomogeneous in depth part of the half-space and this is done in the test examples 3 and 4 as follows.

Test example 3. A semi-elliptical valley rested in a homogeneous half-space subjected to incident longitudinal time-harmonic plane P-wave, see Fig. 2c.

There is no exact solution for this benchmark example. In [57,58] are presented BIEM results for two-dimensional case of a semi-elliptical valley with half-width L, depth h, shape ratio h/L, shear wave velocity in the valley v_s^{valley} situated in a homogeneous half-space with shear wave velocity $v_s^{\text{half-space}}$ and subjected to P- and SV-time-harmonic waves with prescribed incident angle Θ, frequency ω and unit amplitude. Soil is assumed to be isotropic, homogeneous and linear elastic. The contact between valley and half-space is assumed to be perfectly bonded. Comparison between results obtained by Fishman and Ahmad [58] and the BIEM authors' results is presented in Figs. 5a,b in order to evaluate the accuracy of the one of the base tools build up the proposed hybrid technique. Parameters are as follows: dimensionless frequency $\eta = \omega L/\pi v_s$ is 0.5, shape ratio h/L is 0.5, $v_s^{\text{half-space}} = 2v_s^{\text{valley}}$, Poisson's ratio is $\frac{1}{3}$, mass density ratio is $\rho^{\text{valley}}/\rho^{\text{half-space}} = \frac{2}{3}$, incident angle according to axis Oy is $\Theta = 0^\circ$. The displacement amplitude at the free surface is plotted

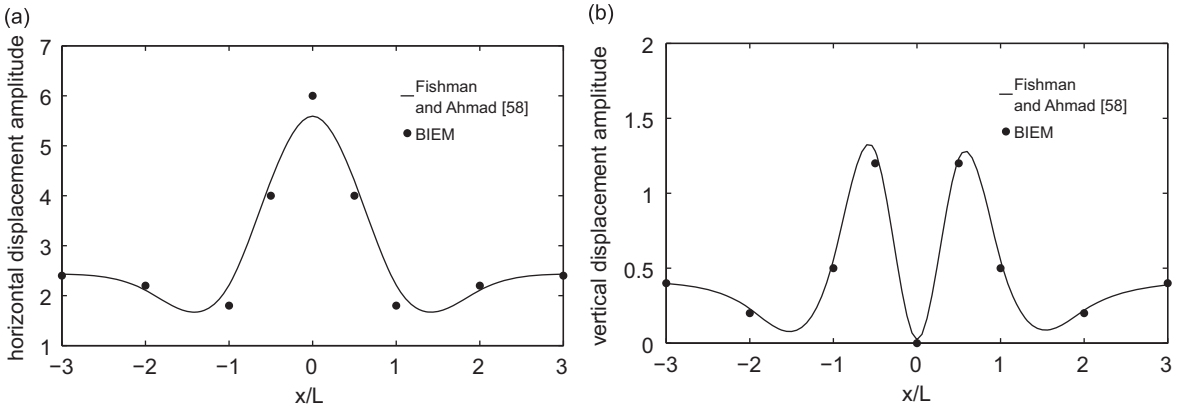

Fig. 5. Displacement amplitudes u_x (case a) and u_z (case b) on the surface of a semi-elliptical valley with shape ratio h/L = 0.5 rested in homogeneous half-space vs dimensionless distance x/L for dimensionless frequency $\eta = 0.5$ at normal incident longitudinal P-wave.

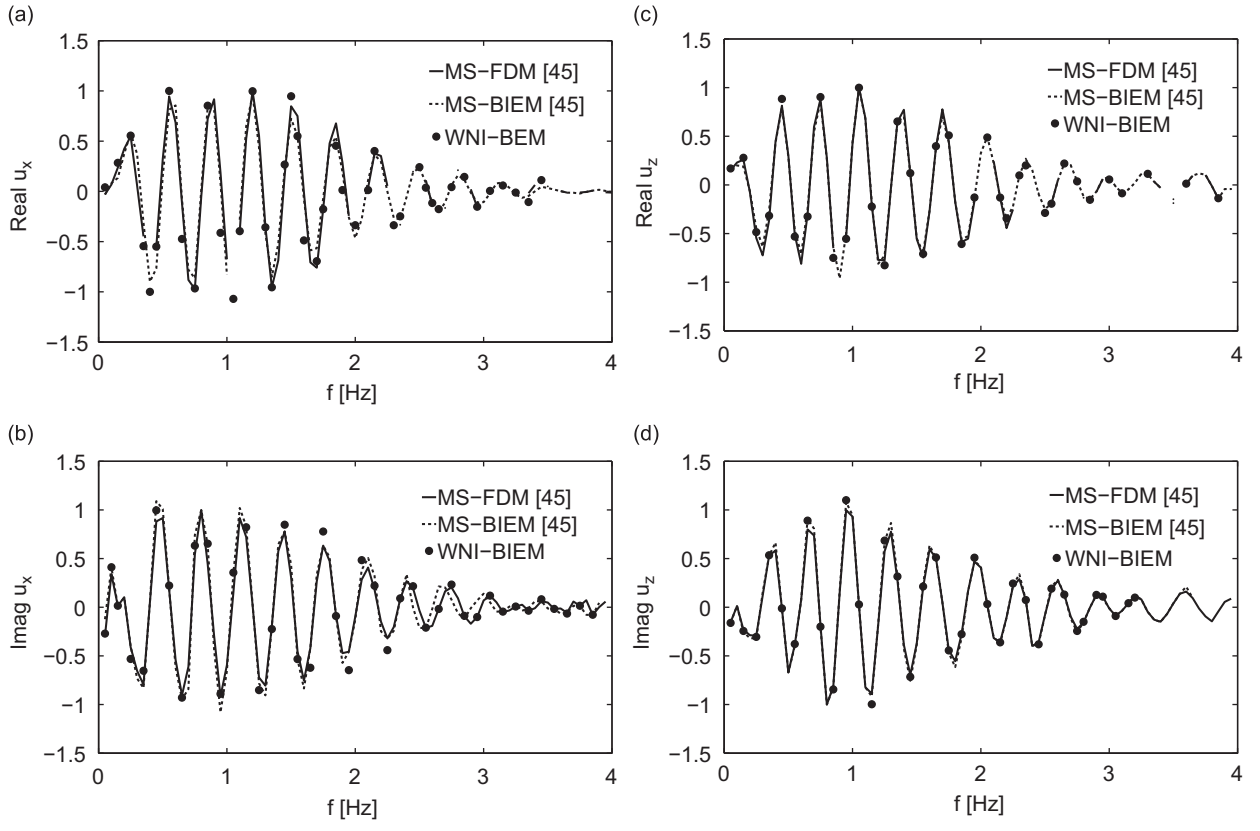

Fig. 6. The real and imaginary part of the displacement components u_x (a, b) and u_z (c, d) obtained by the MS-FDM [45], the MS-BIEM [45] and the WNI-BIEM in the frequency domain at receiver point (0, 30).

vs the dimensionless distance x/L. It is obvious that the obtained authors' results are in agreement with those obtained by Fishman and Ahmad in [58].

Test example 4. Seismic response of a finite local geological region with relief peculiarities and non-parallel layers rested in an inhomogeneous-in-depth half-space presented by a stack of flat horizontal layers with a seismic source in one of them.

The geometry of this benchmark example is given in Fig. 2d. The finite local soil stratum Ω_{LGR} is situated in the first layer of the half-space and it has three layers with non-parallel interfaces. There is a free-surface relief in the form of a semi-circular canyon of radius $r=A=30$ m. The coordinates of the points indicating the geometrical boundaries of the layers are: $T_0(30,0)$; $T_3(60,0)$; $T_2(90,0)$; $T_1(100,0)$; $P_0(-30,0)$; $P_3(-60,0)$; $P_2(-90,0)$; $P_1(-100,0)$; $L_1(110,270)$; $R_1(-110,270)$;

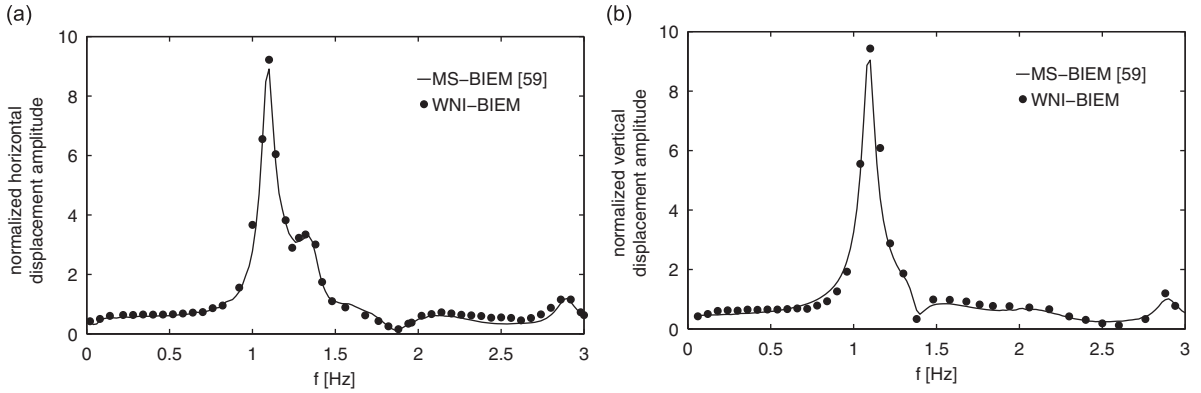

Fig. 7. Normalized displacement components obtained by MS-BIEM [59] and WNI-BIEM in the frequency domain at receiver point $(-30, 0.0)$.

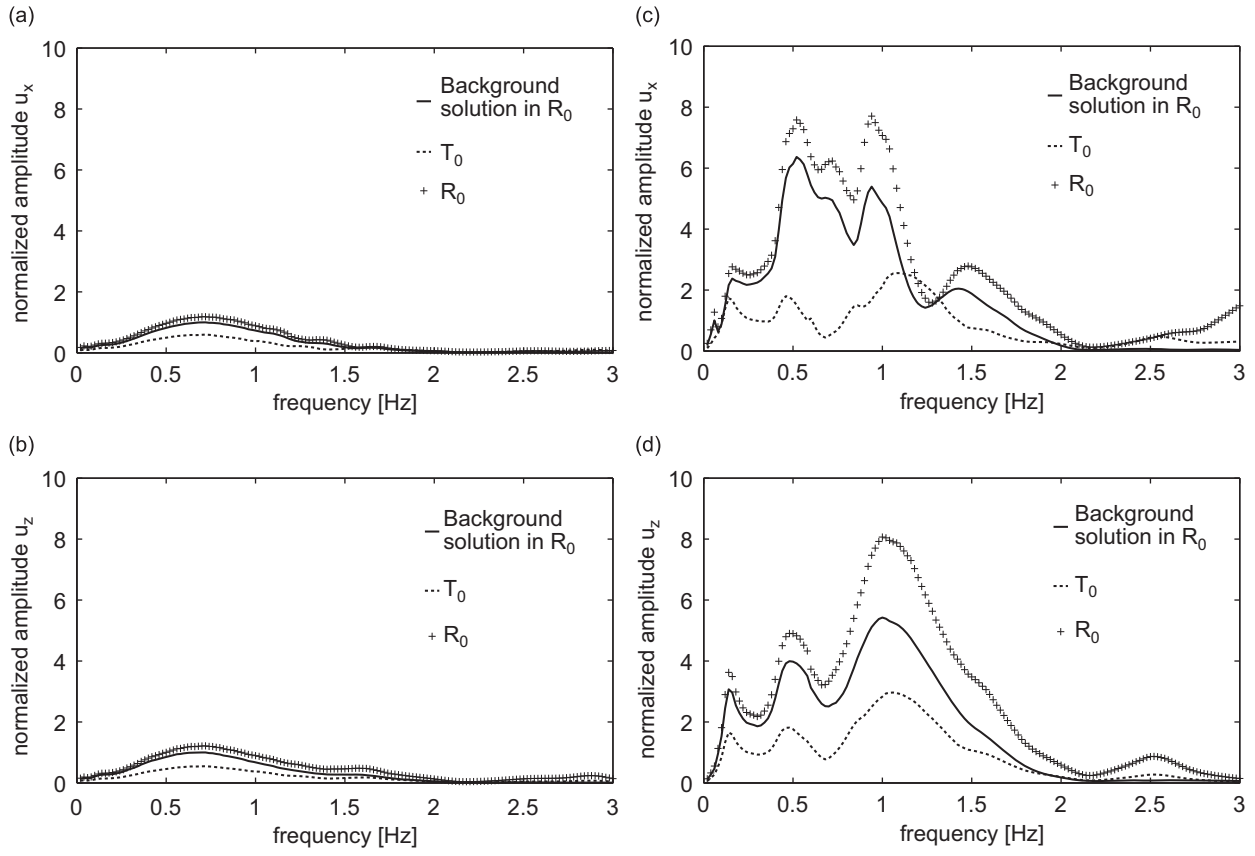

Fig. 8. Normalized displacement amplitudes vs frequency at receivers $T_0(30,0)$ and $R_0(0,30)$ for buried line seismic source at depth of 6 km and for two wave paths: (a) and (b) wave path 1; (c) and (d) wave path 2.

$L_2(90,180)$; $R_2(-90,180)$; $L_3(60,90)$; $R_3(-60,90)$. The mechanical properties of the background model are presented in Table 1a. The density ρ, longitudinal α and shear β wave velocities of the layers in Ω_{LGR} are as follows: $\rho_3 = 2400\,\mathrm{kg/m^3}$; $\alpha_3 = 5000\,\mathrm{m/s}$; $\beta_3 = 2900\,\mathrm{m/s}$; $\rho_2 = 2800\,\mathrm{kg/m^3}$; $\alpha_2 = 4500\,\mathrm{m/s}$; $\beta_2 = 2430\,\mathrm{m/s}$; $\rho_1 = 2800\,\mathrm{kg/m^3}$; $\alpha_1 = 5500\,\mathrm{m/s}$; $\beta_1 = 2970\,\mathrm{m/s}$. An instantaneous source corresponding to a pure double couple is in the half-space at depth of 2 km and epicentre distance of 10 km. The dip angle δ is 60°, the rake angle θ is 90° and the strike angle ϕ is 30°. The seismic moment of the source is taken to be 1×10^{13}N m. The discretization mesh consists of 170 quadratic boundary elements and the discretization along the boundaries T_1L_1, L_1R_1, R_1P_1 and T_0P_0 is the same as those at solution of the test examples 1 and 2. The same numerical example was solved in [45] by the usage of other two hybrid techniques as the modal summation-finite difference method (MS-FDM) and the modal summation-BIEM (MS-BIEM). The numerical results of the proposed WNI-BIE method are compared with the results presented in [45] and obtained by the usage of two different hybrid numerical schemes. Figs. 6a–d show the comparison of the solutions for normalized displacement components at the receiver point (0,30) (the bottom of the canyon) obtained by three different hybrid computational tools. The normalization is done by the maximal absolute value of the corresponding displacement component. These figures show very close solutions in the frequency domain. The shapes of the wavelets coincide for all three techniques and the differences in amplitudes are of the order of average percentage error about 8%. The test example with the same geometry is solved in [59] by the hybrid MS-BIEM with the data for the case study of the capital city of Bulgaria, Sofia. The bedrock model is with mechanical characteristics for the Sofia region [61], the seismic source is with the following characteristics: the dip angle δ is 44°, the rake angle θ is 309°, the strike angle ϕ is 21°, the magnitude is 3.7, the source depth is 12 km and the epicentre distance is 20 km. The mechanical constants of the layers in the local geological region are taken from [59] for a sandstone formation to: $\rho_3 = 1749\,\mathrm{kg/m^3}$; $\alpha_3 = 1582\,\mathrm{m/s}$; $\beta_3 = 969\,\mathrm{m/s}$; $\rho_2 = 1696\,\mathrm{m/s}$; $\alpha_2 = 486\,\mathrm{m/s}$; $\beta_2 = 300\,\mathrm{m/s}$; $\rho_1 = 2650\,\mathrm{kg/m^3}$; $\alpha_1 = 5700\,\mathrm{m/s}$; $\beta_1 = 3290\,\mathrm{m/s}$. Figs. 7a,b present a comparison between normalized seismograms obtained by both hybrid methods WBI-BIEM and MS-BIEM at receiver $(-30, 0)$ (the edge of the canyon). Normalization is made with respect to the amplitude of the corresponding displacement component of the bedrock reference regional model. Fig. 7 demonstrates that the results for the seismic response obtained by both hybrid methods are very close. The obtained results in the validation study show that the proposed hybrid WNI-BIEM works with high accuracy and we will use it in our simulation study presented in the following section. The created FORTRAN program code has the following parameters: at a fixed frequency the CPU time is 7 min, the peak memory is 3524K, for AMD Athlon (TM), 1.60 GHz, 512 MB RAM.

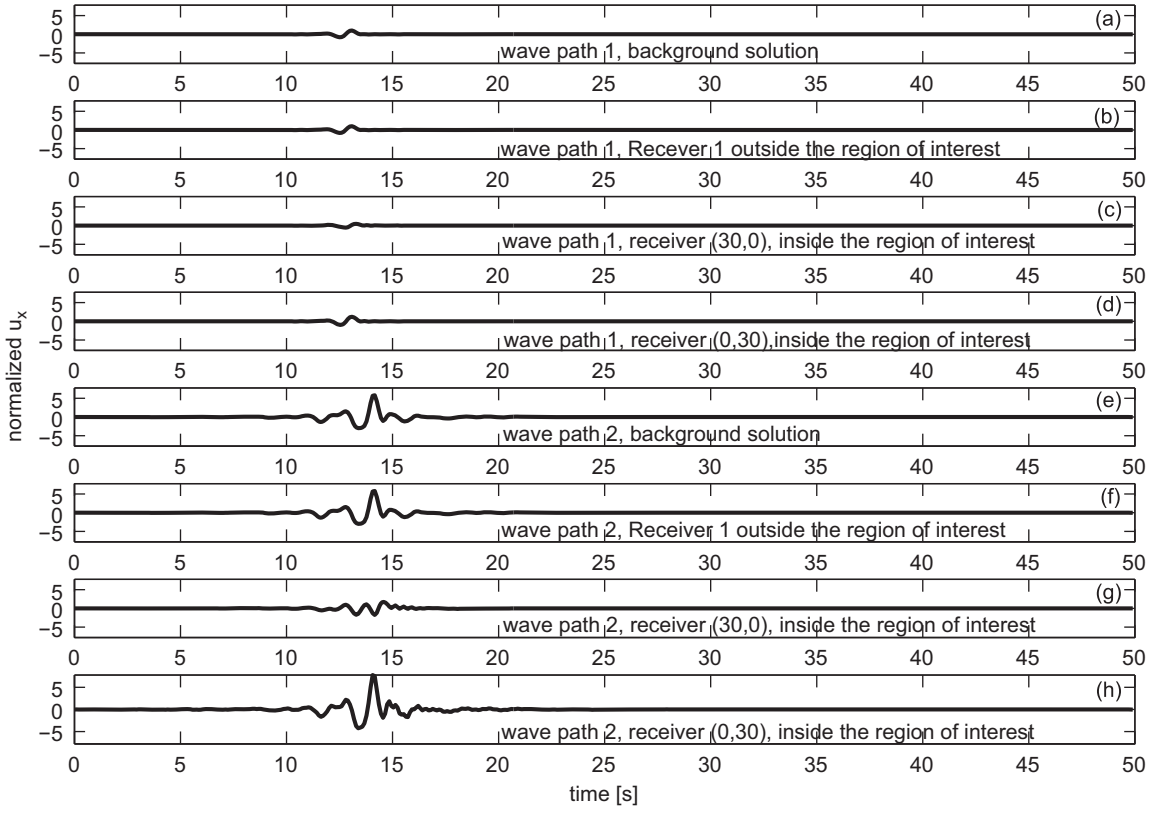

Fig. 9. Normalized horizontal displacement vs time at receivers $T_0(30,0)$ and $R_0(0,30)$ for buried line vertical seismic source at $x=2$ km, depth of $z=6$ km, and for two wave paths: (a)–(d) wave path 1; (e)–(h) wave path 2.

5. Numerical simulations

In order to illustrate the efficiency of the proposed hybrid method, the response of a multilayered region with geometry given in the test example 4 (Fig. 2d) is analyzed. Three types of the free-surface geometry relief are considered: (a) flat model; (b) semi-circle canyon with radius $r=A=30$ m; (c) semi-circle hill with radius $r=A=30$ m. The mechanical properties of the finite geological region are given in Table 2. The aim of the simulation study is to demonstrate that the synthetic signals, obtained through the proposed hybrid WNI-BIEM, depend on: (a) wave path inhomogeneity; (b) relief existence on the free surface; (c) mechanical properties of the local finite soil stratum and lateral inhomogeneity of the local geological region; (d) seismic source characteristics. Each one of these effects is considered and discussed below.

5.1. Sensitivity of the obtained synthetic seismic signals to the wave path properties

Canyon relief on the free surface of the local geological region is considered. Synthetic seismograms are obtained at two different wave paths 1 and 2 with properties given in Table 1a, b. The mechanical properties of the finite local stratum are given in Table 2. The main properties of the seismic source A are: a buried vertical line source is defined at $x=2$ km and a depth of 2 km or 6 km. The source term was assumed as a Ricker wavelet of the second order with time duration of 1.28 s and with an unit load. Two receiver points are considered: receiver $T_0(30,0)$ is the edge of the canyon and receiver $R_0(0,30)$ is the bottom of the canyon. Figs. 8a,b present the displacement amplitudes vs frequency at both receivers in the case of wave path 1. Figs. 8c,d display the same curves, but in the case of wave path 2. A comparison between the displacements in Figs. 8a,b with those in Figs. 8c,d shows the influence of wave path properties on the free surface's seismic signals. Fig. 8 demonstrates very clearly the existence of site effects and also their dependence on the type of the wave path inhomogeneity. The effect of site amplification is stronger in the case of wave path 2. The discussed simulation results demonstrate the sensitivity of the wave field to the wave path specific properties. Figs. 9 and 10 present the synthetic displacement signals in time domain. In both figures, the cases (a) and (e) present the background 1D solution, the cases (b) and (f) show the wave field in the Receiver 1 outside the excitation region, while the cases (c), (d), (g) and (h) show the wave field inside the region of interest. Receiver 1 is the first boundary node on the free surface outside the excitation region. As can be seen, the total wave field outside the region of interest replicates the background solution that demonstrate zero values of the scattered wave field outside the excitation region and this means that the minimal information about the interaction between the scattered wave field and the structural features deeper than

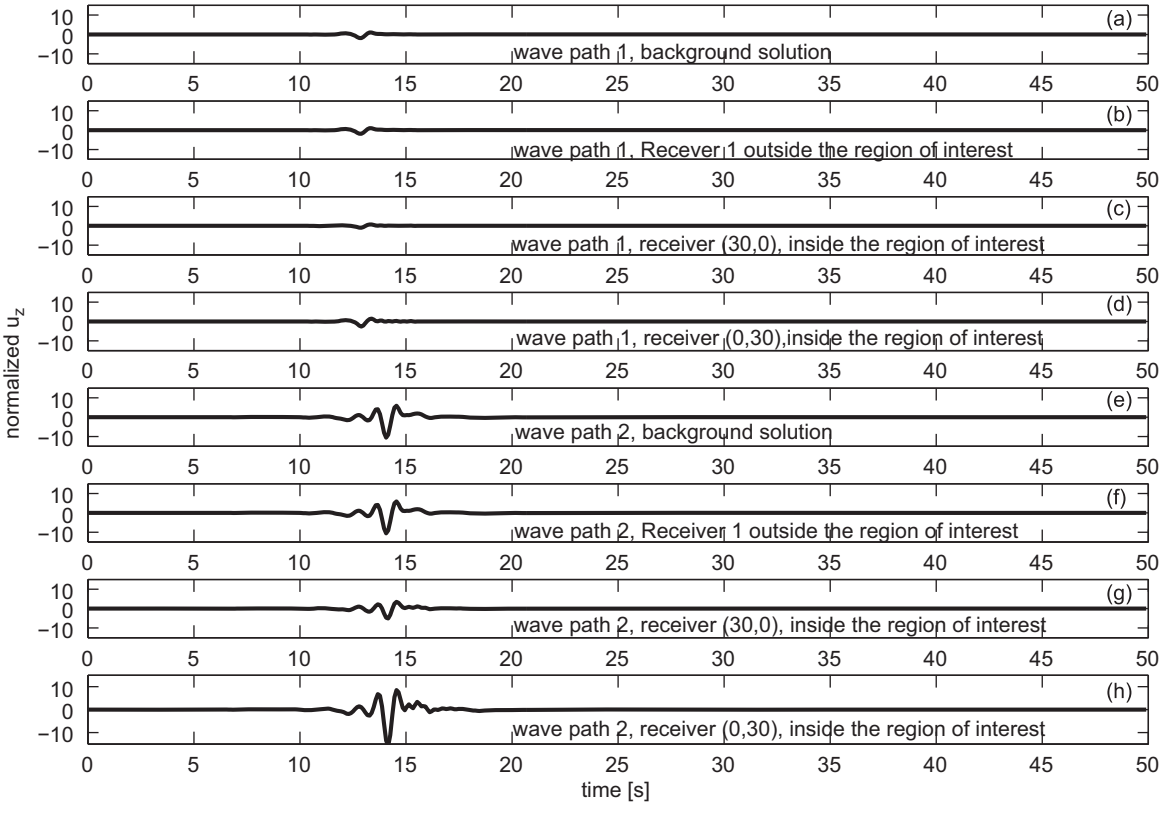

Fig. 10. Normalized vertical displacement vs time at receivers $T_0(30,0)$ and $R_0(0,30)$ for buried line vertical seismic source at $x=2$ km, depth of $z=6$ km, and for two wave paths: (a)–(d) wave path 1; (e)–(h) wave path 2.

the excitation region have been lost. Normalization in Figs. 8–10 is made with respect to the maximal amplitude of the corresponding displacement component, synthesized for the bedrock reference model (wave path 1). All results confirm the conclusion that wave path properties can dramatically change the character of the seismic signals.

5.2. Sensitivity of the obtained synthetic seismic signals to the free surface relief of the local geological region

The effects of surface geology can greatly enlarge the site response, exerting an important influence on the distribution of damage observed during earthquakes. In [62–64], the need of incorporating or reviewing parameters related to the local topography to account for topographical effects in the seismic response is pointed out. The role of lateral heterogeneity in

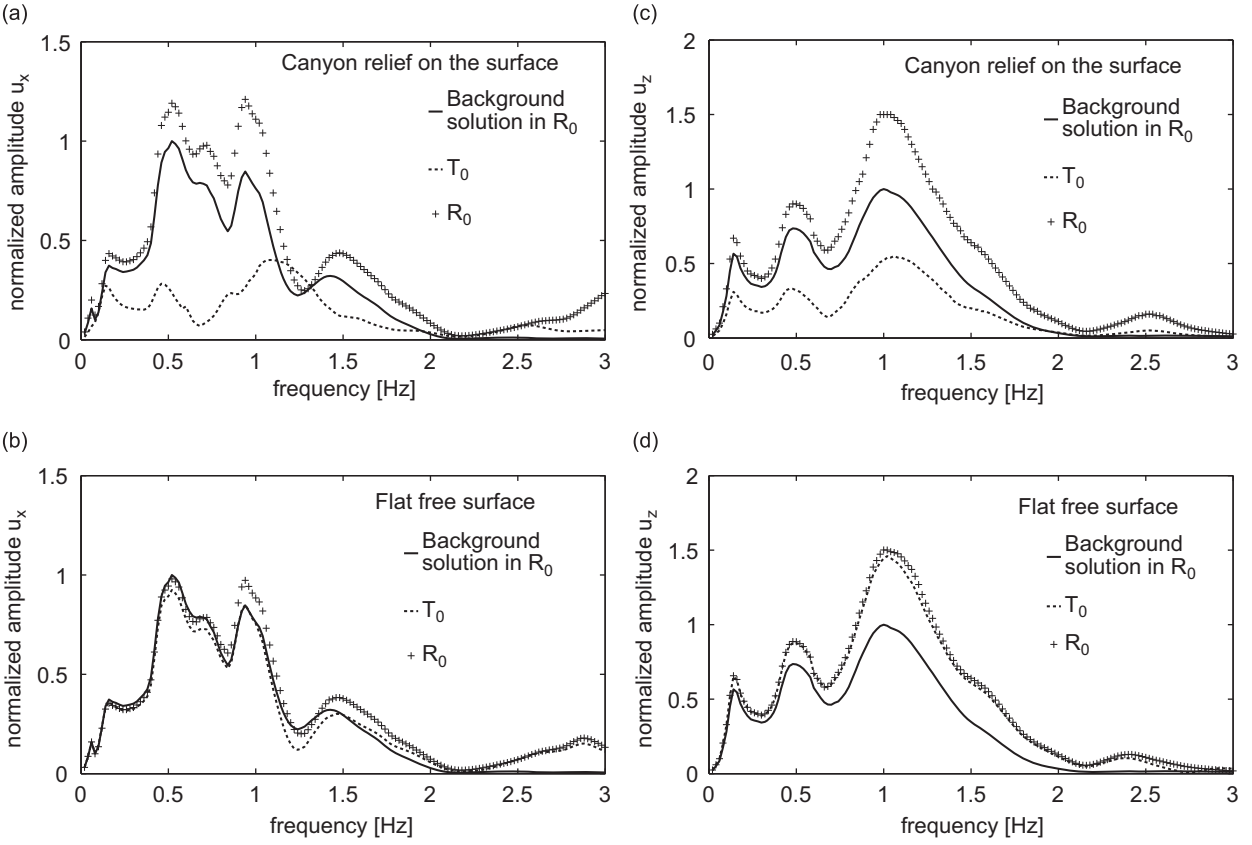

Fig. 11. Normalized displacement amplitude vs frequency at receivers $T_0(30,0)$, $R_0(0,30)$ on the free surface without and with canyon relief in the case of a buried line vertical seismic source at $x=2$ km, depth of $z=6$ km and wave path 2.

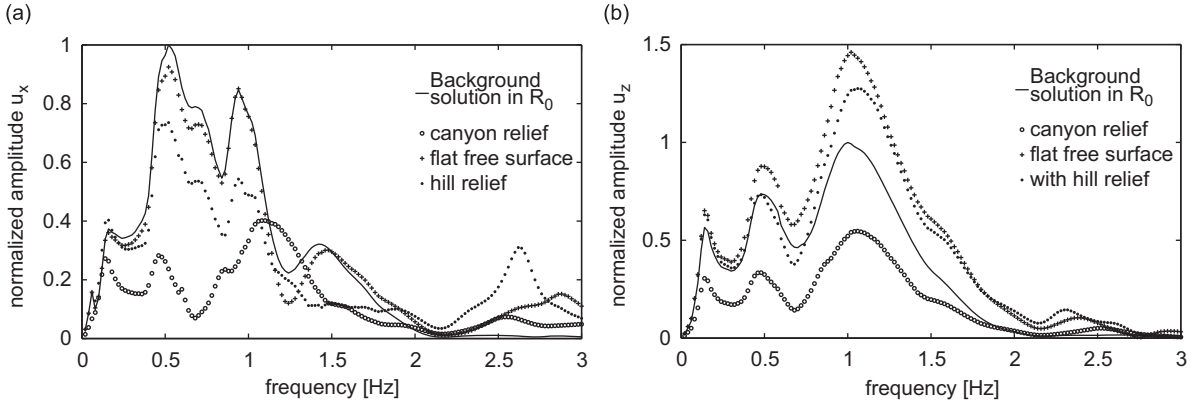

Fig. 12. Normalized displacement amplitude vs frequency at receiver $T_0(30,0)$ on the free surface without and with relief (canyon or hill) in the case of a buried line vertical seismic source at $x=2$ km, depth of $z=6$ km and wave path 2.

site effects, especially in small and shallow sedimentary basins has been observed in Coachella valley in California by [65], Parkway in New Zealand by [66], Colfiorito in Italy by [67,68]. The WNI-BIEM can show the influence of the relief on the computed seismic signals. Figs. 11 and 12 reveal the sensitivity of the seismic signals to the free surface relief.

The synthetic seismograms shown in Figs. 11 and 12 are obtained at wave path 2 and seismic source A at a depth of 6 km. The mechanical properties of the local soil region are given in Table 2. Three types of the free surface geometry are considered: (a) flat surface; (b) canyon relief; (3) hill-like relief, correspondingly. Normalization in Figs. 11–17 is made

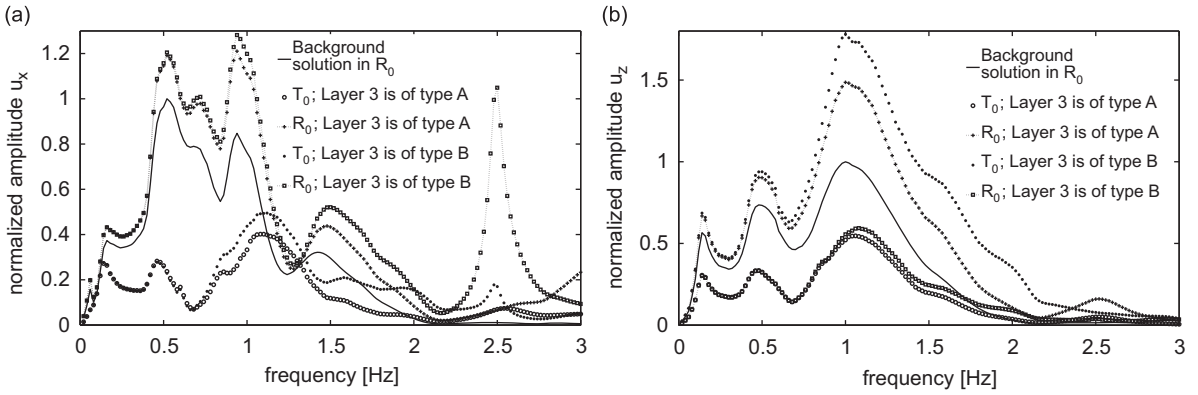

Fig. 13. Normalized displacement amplitude vs frequency at receivers $T_0(30,0)$, $R_0(0,30)$ on the free surface with canyon in the case of a buried line vertical seismic source at $x=2$ km, depth of $z=6$ km and wave path 2.

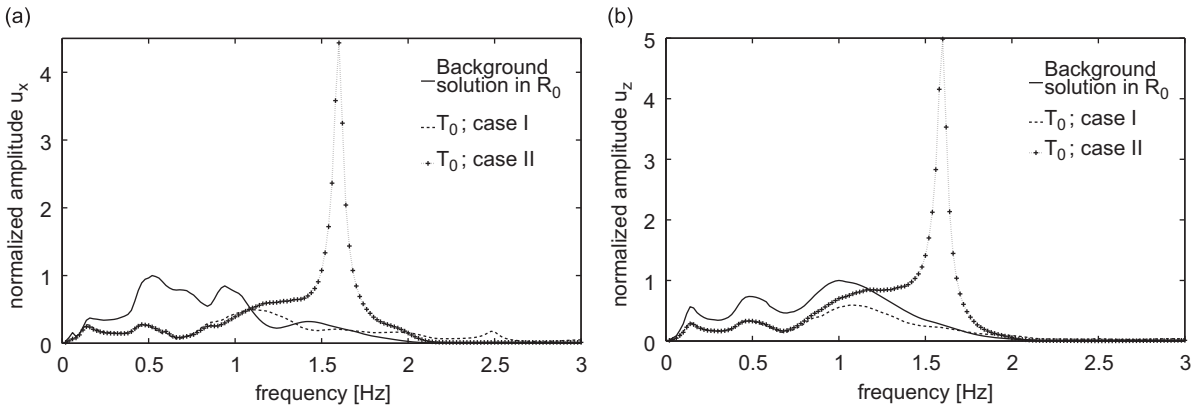

Fig. 14. Normalized displacement amplitude vs frequency at receiver $T_0(30,0)$ on the free surface of the local geological region with a semi-circle canyon in the case of a buried line vertical seismic source at $x=2$ km, depth of $z=6$ km and wave path 2 for two different cases I and II of the mechanical properties of the local soil stratum.

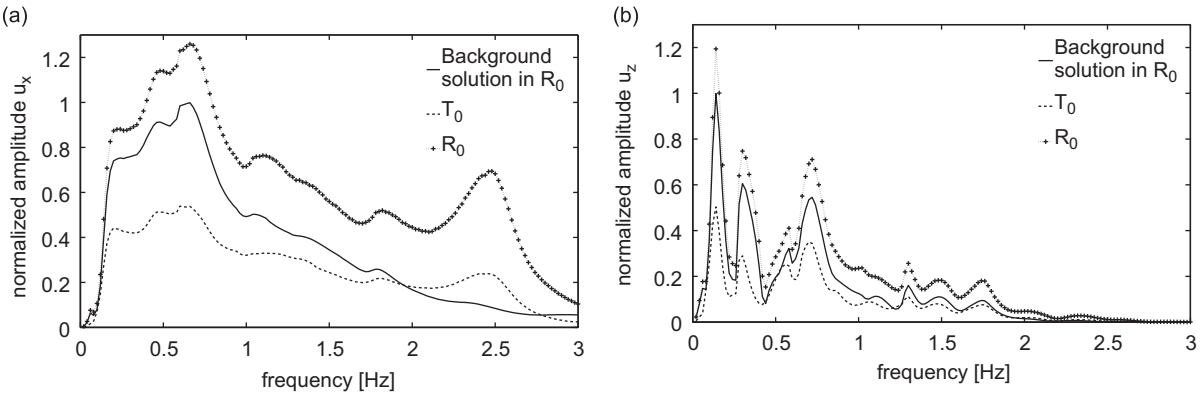

Fig. 15. Normalized displacement amplitude vs frequency at receivers $T_0(30,0)$, $R_0(0,30)$ on the free surface of the local geological region with a semi-circle canyon, at wave path 2 and a buried line vertical seismic source at $x=2$ km and depth of: (a) 2 km; (b) depth 6 km.

with respect to the maximal amplitude of the corresponding displacement component, synthesized for the bedrock reference model (wave path 2). Figs. 11a,b show the horizontal component of displacement amplitude in the case of local multilayered region with canyon relief and with flat free surface, correspondingly. Figs. 11c,d show the vertical component of displacement amplitude versus frequency for free surface with and without canyon relief. The discussed results reveal that the site effects are much stronger in the case of relief on the free surface, while in the case of flat free surface there is no clear presence of the site amplification. This can be explained with the complex diffraction wave picture in the case of canyon relief, i.e. with the well known edge effects. Figs. 12a,b compare the displacement amplitudes at receiver (30,0)

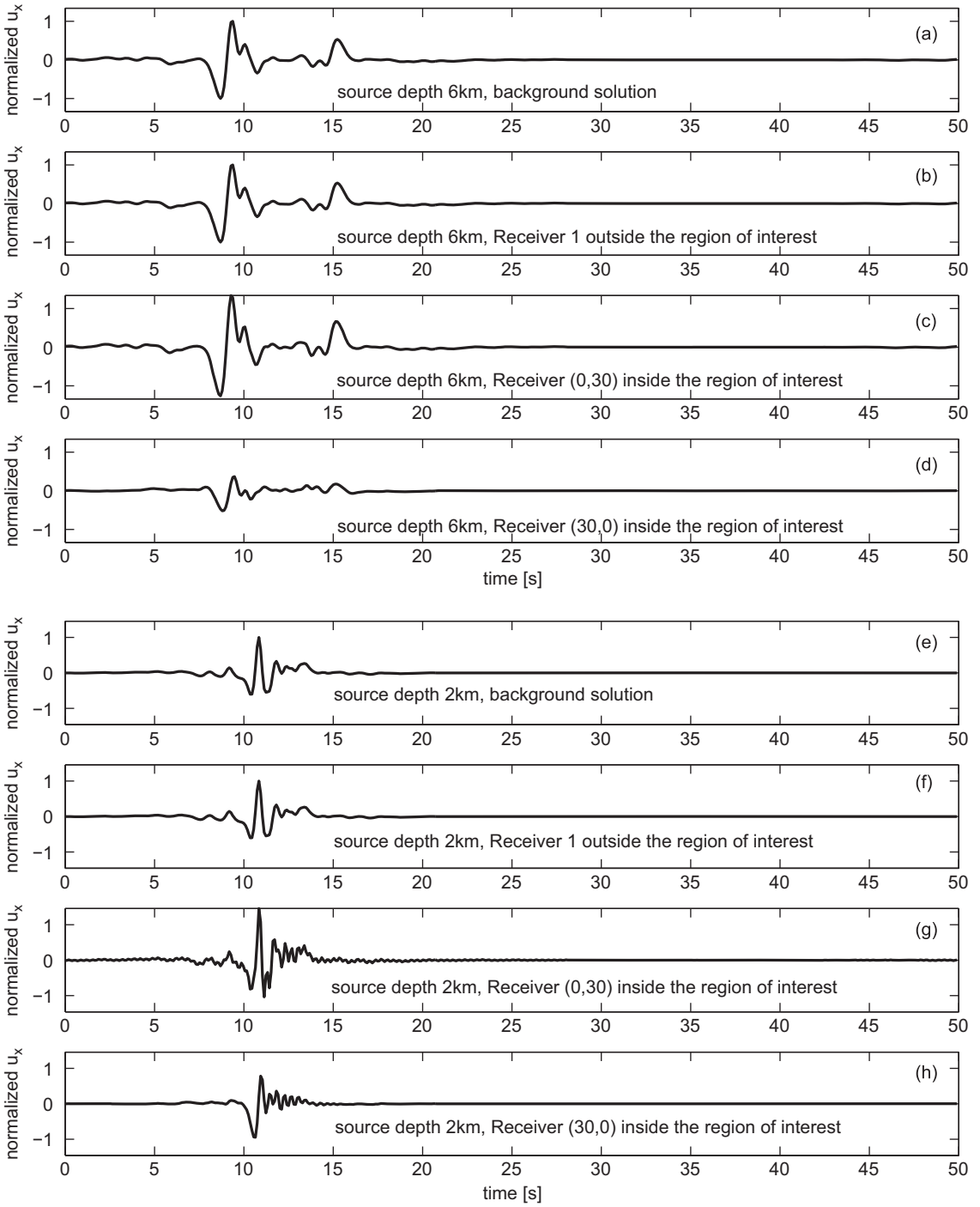

Fig. 16. Normalized horizontal displacement vs time at receivers $T_0(30,0)$ and $R_0(0,30)$. The seismic source is a double couple, situated at x=2 km and depth of: (a)–(d) z=6 km; (e)–(h) z=2 km.

(the edge of the canyon) on the free, horizontal surface and the free surface with relief (canyon or hill). In the case of canyon relief the displacement amplitudes are the smallest one, while in the case of the free, horizontal surface they are the greatest one. The complex diffraction wave picture in the case of relief peculiarities is responsible for this behavior.

5.3. Sensitivity of the obtained synthetic seismic signals to the mechanical properties of the local geological region

The mechanical properties of the local soil stratum play an important role on the specific character of the seismic signal. Fig. 13 shows displacement amplitudes at receiver $T_0(30,0)$ and receiver $R_0(0,30)$ vs frequency, at seismic source A at a

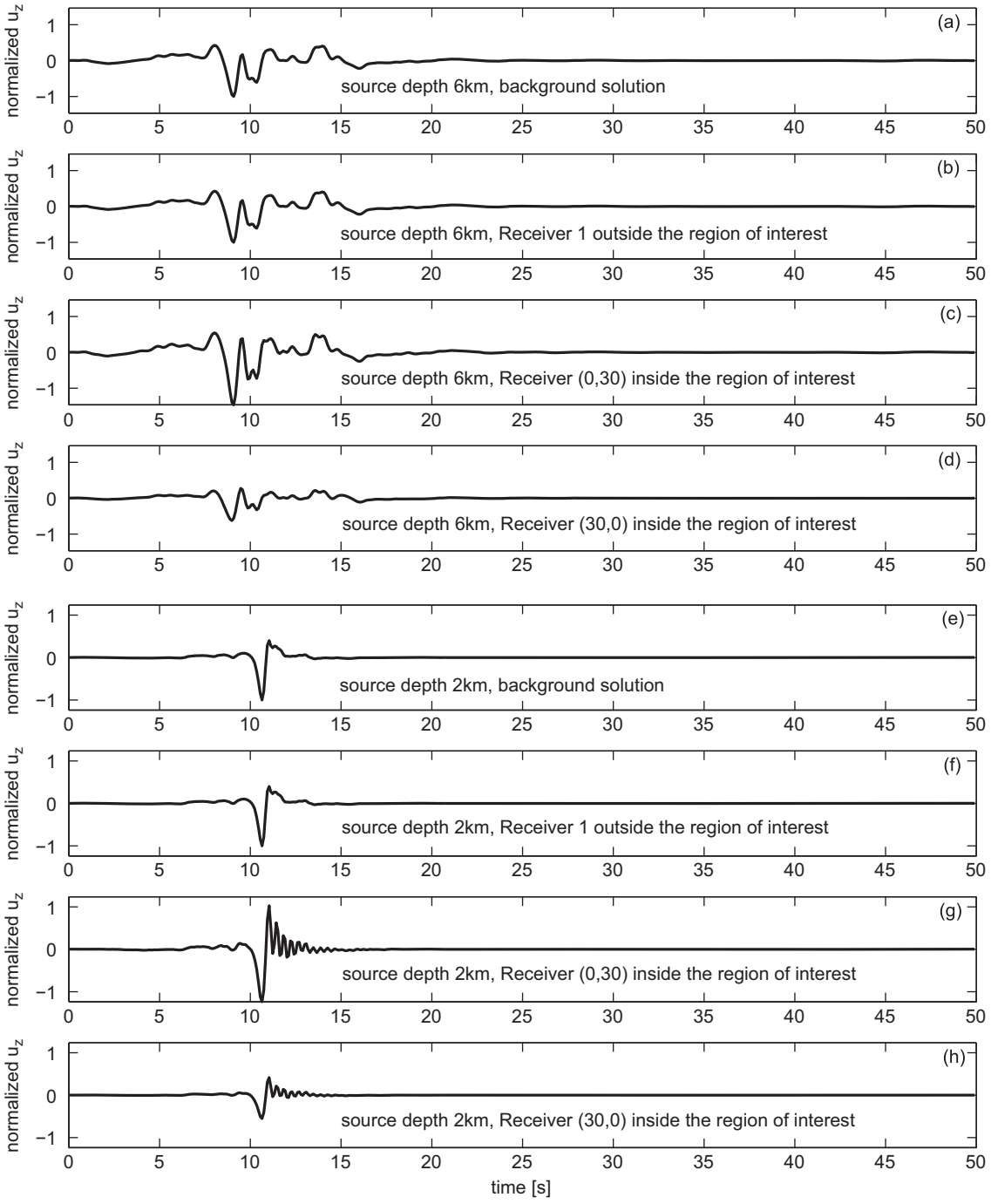

Fig. 17. Normalized vertical displacement vs time at receivers $T_0(30,0)$ and $R_0(0,30)$. The seismic source is a double couple, situated at $x=2$ km and depth of: (a)–(d) $z=6$ km; (e)–(h) $z=2$ km.

depth of 6 km and wave path 2. The mechanical properties of the local geological region are presented in Table 2. The third soil layer is of *type A* ($\beta_3 = 800\,\mathrm{m/s}$, $\alpha_3 = 1500\,\mathrm{m/s}$) or of *type B* ($\beta_3 = 500\,\mathrm{m/s}$, $\alpha_3 = 900\,\mathrm{m/s}$). Fig. 14 compares seismic signals obtained at receiver T_0 for two cases of mechanical properties of the finite soil profile: (a) case I — material characteristics are as those given in Table 2; (b) case II — second and third layers change their positions, i.e. second layer is with the properties of the third layer and vice versa . This leads to a complete different character of the synthetic seismograms. Figs. 13 and 14 reveal how important are the mechanical properties of the local seismic region for the characteristic peculiarities of the obtained wave signals during earthquake.

5.4. Sensitivity of the obtained synthetic seismic signals to the seismic source properties

The synthetic seismograms are obtained for seismic source B at two different depths. The rest of the data is fixed, it is considered wave path 2 and canyon relief on the free surface, while the mechanical properties of the local soil region are given in Table 2. The seismic source B used for the simulation study is the so-called double couple source. The time dependency of the seismic moment $M_0(t)$ is defined after [69]. As source parameters were chosen scalar seismic moment $M_0 = 5.98 \times 10^{14}\,\mathrm{N\,m}$, corner frequency $f_c = 5.0\,\mathrm{Hz}$, strike angle $\varphi = 151^\circ$, dip angle $\delta = 83^\circ$ and rake angle $\theta = 7^\circ$. To show the effects of different source depths this source is implemented in $x = 2\,\mathrm{km}$ and a depth of 2 km or 6 km. Figs. 15–17 demonstrate in frequency and in time domain, respectively, how sensitive are the synthetic signals to the depth of the seismic source. The discussed numerical results in this item show that the synthetic signals and the site effects depend on all essential components of the seismic wave path: seismic source located in the half-space, inhomogeneous wave path from the source to the local geological region plus the lateral inhomogeneous finite local stratum with its complex mechanical and geometrical peculiarities. The proposed, developed and validated hybrid analytically numerical tool has the possibility to account for all these important components of the seismic wave.

6. Concluding remarks

Efficient hybrid wavenumber integration-boundary integral equation method is developed, validated and applied in simulation studies. The hybrid approach combines analytical WNIM and numerical BIEM. PROS and CONS of the proposed hybrid tool are as follows: (a) it is possible to treat many soil layers due to the effective combination of both methods; (b) wave field can be evaluated for small and large distances; (c) body and surface waves are considered; (d) BIEM allows modeling of complex geometry, relief existence, non-parallel layering, inhomogeneities like cracks, inclusions, etc.; (e) capability to obtain seismograms, velocigrams and accelerograms, also response spectra, that account for the properties of the earthquake source, inhomogeneous wave path and laterally varying local geological region; (f) potential to account for geological regions with more complex mechanical behavior as anisotropy, poroelasticity, non-elasticity, etc.; (g) most of the papers in the literature take into account either one or two of the physical mechanisms controlling the seismic wave, while the hybrid WNI-BIEM has the potential to study simultaneously the combined effects of different physical properties of the system: seismic wave-geological media; (k) special attention is needed at high frequencies and for very soft soil layers, where the wavelength is small. It is clear that to reach high-numerical accuracy in these cases a very fine BEM mesh

Table 1
(a) The properties of the layered half-space (wave path 1); (b) the properties of the layered half-space (wave path 2).

Number of soil layer Γ_i	Thickness (km)	Depth (km)	Density ρ_1 (kg/m^3)	Shear wave velocity β_i (m/s)	Longitudinal wave velocity α_i (m/s)
(a)					
1	5.0	5.0	2750	3500	6100
2	8.0	13.0	2900	3600	6200
3	4.0	17.0	3200	4100	7650
4	2.0	19.0	3200	4200	7500
5	2.0	21.0	3200	4200	7650
6	2.0	23.0	3200	4300	7800
7	5.0	28.0	3300	4350	8000
8	22.0	50.0	2900	3800	6800
Seismic bed	∞	∞	3350	4600	8200
(b)					
1	0.35	0.35	2100	1400	2400
2	0.65	1.0	2200	1400	2400
3	1.5	2.5	2300	1400	2400
4	1.0	3.5	2400	1400	2400
5	1.5	5.0	2500	2200	3800
6	2.0	7.0	2600	2550	4500
7	5.0	12.0	2650	3100	5400
8	13.0	25	2750	3500	6200
9	10.0	35.0	2900	4200	7500
Seismic bed	∞	∞	3350	4600	8200

Table 2
The properties of the local geological region.

Number of soil layer	Density ρ_1 (kg/m^3)	Shear wave velocity β_i (m/s)	Longitudinal wave velocity α_i (m/s)
3	1800	800	1500
2	2000	1000	1700
1	2000	1400	2400

has to be used, respective this leads to high values of CPU time and memory; (l) it is necessary to establish the limits and possibilities of the proposed hybrid technique for each new seismic scenario and to this aim one-dimensional simulation experiment allows us to consider the WNIM result as one of the reference benchmark examples.

The seismic signal, obtained by the hybrid technique, can be used as a necessary base for solution of the following important geotechnical and civil engineering problems: (a) seismic wave propagation with accounting for the more complex mechanical behavior of the soil (b) soil–structure interaction and its effects on the dynamics of structures during earthquake; (c) solution of inverse problems for dynamic site characterization and identifying the soil profiles.

Acknowledgements

The authors acknowledge the support of the NATO under the Grant number CLG982064 and the *R&D*-Programme GEOTECHNOLOGIEN funded by the German Ministry of Education and Research (BMBF) and German Research Foundation (DFG), Grant 03G0636B with the publication no. GEOTECH - 320.

References

[1] F.J. Sanchez-Sesma, Strong ground motion and site effects, in: S.A. Anagnostopoulos, D. Beskos (Eds.), *Computer Analysis and Design of Earthquake Resistant Structures*, Computational Mechanics Publications, Southampton, 1996, pp. 201–239.
[2] V.M. Babich, *Ray Method for the Computation of the Intensity of Wavefronts*, Nauka, Moscow, 1956.
[3] C.H. Chapman, R. Drummond, Body-wave seismograms in inhomogeneous media using Maslov asymptotic theory, *Bulletin Seismological Society of America* 72 (1982) 277–317.
[4] N. Frazer, Quadrature of wave number integrals, in: D.J. Doornbos (Ed.), *Seismological Algorithms*, Academic Press, 1988.
[5] V. Cerveny, M.M. Popov, I. Psencik, Computation of seismic wave fields in inhomogeneous media-Gaussian beam approach, *Geophysical Journal of the Royal Astronomical Society* 70 (1982) 109–128.
[6] Y.H. Pao, R.G. Gajewski, The generalized ray theory and transient response of layered elastic solids, in: R.N. Thurston, W.P. Mason (Eds.), *Physical Acoustics*, Academic Press, New York, 1977, pp. 183–265.
[7] J.E. Gubernatis, E. Domany, J.A. Krumhansl, M. Huberman, Born approximation in the theory of scattering of elastic waves, *Journal of Applied Physics* 48 (1977) 2812–2819.
[8] B.L.N. Kennett, *Seismic Wave Propagation in Stratified Media*, vol. I, Cambridge University Press, 1983.
[9] Y. Hisada, An efficient method for computing Green's functions for a layered half-space with sources and receivers at close depths (Part 1), *Bulletin Seismological Society of America* 84 (5) (1994) 1456–1472.
[10] Y. Hisada, An efficient method for computing Green's functions for a layered half-space with sources and receivers at close depths (Part 2), *Bulletin Seismological Society of America* 85 (4) (1995) 1080–1093.
[11] L. Burdik, J. Orcutt, A comparison of the generalized ray and reflectivity methods of waveform synthesis, *Geophysical Journal of the Royal Astronomical Society* 58 (1979) 261–278.
[12] Z.S. Alterman, F.C. Karal, Propagation of elastic waves in layered media by finite difference methods, *Bulletin of the Seismological Society of America* 58 (1968) 367–398.
[13] D. Fah, P. Suhadolc, G.F. Panza, Estimation of strong ground motion in laterally heterogeneous media: modal summation-finite differences, *Proceedings of the 9th European Conference of Earthquake Engineering*, Moscow, USSR, vol. 4A, 11–16 September 1990, pp. 100–109.
[14] D. Fah, A Hybrid Technique for the Estimation of Strong Ground Motion in Sedimentary Basins, PhD Thesis, ETH Nr. 9767, Swiss Federal Institute of Technology, Zurich, 1992.
[15] D. Fah, P. Suhadolc, G.F. Panza, Variability of seismic ground motion in complex media: the case of a sedimentary basin in the Fruili Italy area, *Journal of Applied Geophysics* 30 (1993) 131–148.
[16] D. Fah, P. Suhadolc, St. Muller, G.F. Panza, A hybrid method for the estimation of ground motion in sedimentary basins: quantitative modelling for Mexico City, *Bulletin of the Seismological Society of America* 84 (2) (1994) 383–399.
[17] J. Zahradnik, P. Moczo, Hybrid seismic modelling based on discrete wave number and finite difference methods, *PAGEOPH* 148 (1/2) (1996) 21–38.
[18] P. Moczo, E. Bystricky, J. Kristek, M. Carcione, M. Bouchon, Hybrid modelling of P-SV seismic motion at inhomogeneous viscoelastic topographic structures, *Bulletin of the Seismological Society of America* 87 (5) (1997) 1305–1323.
[19] I. Oprsal, M. Pakzad, V. Plicka, J. Zahradnik, Ground motion simulation by hybrid methods, in: K. Irikura, K. Kudo, H. Okada, T. Sasatani, (Eds.), *The Effects of Surface Geology on Seismic Motion, Proceedings of ESG'98*, December 1–3, 1998, Yokohama, Japan, Vol. 2, Balkema, Rotterdam, 1998, pp. 955–960. ISBN 9058090337.
[20] I. Oprsal, V. Plicka, J. Zahradnik, Kobe simulation by hybrid methods, in: K. Irikura, K. Kudo, H. Okada, T. Sasatani, (Eds.), *The Effects of Surface Geology on Seismic Motion, Proceedings of ESG'98*, December 1–3, 1998, Yokohama, Japan, Vol. 3, Balkema, Rotterdam, 1999, pp. 1451–1456, ISBN 9058090337.
[21] I. Oprsal, J. Zahradnik, Three-dimensional finite difference method and hybrid modelling of earthquake ground motion, *Journal of Geophysical Research* 107 (B8) (2002) 16 10.1029/2000JB000082.
[22] J. Bielak, P. Christiano, On the effective seismic input for nonlinear soil structure interaction systems, *Earthquake Engineering Structural Dynamics* 12 (1984) 107–119.
[23] J. Bielak, K. Loukakis, Y. Hisada, Ch. Yoshimura, Domain reduction method for three-dimensional earthquake modelling in localized regions. Part I: theory, *Bulletin of the Seismological Society of America* 93 (2) (2003) 817–824.
[24] J.O.A. Robertsson, C.H. Chapman, An efficient method for calculating finite-difference seismograms after model alterations, *Geophysics* 65 (2000) 907–918.

[25] I. Oprsal, C. Matyska, K. Irikura, The source-box wave propagation hybrid methods: general formulation and implementation, *Geophysical Journal International* 176 (2009) 555–564.
[26] P.Y. Bard, M. Bouchon, The seismic response of sediment-filled valleys. Part I. The case of incident SH waves, *Bulletin of the Seismological Society of America* 70 (1980) 1263–1286.
[27] P.Y. Bard, M. Bouchon, The seismic response of sediment-filled valleys. Part II. The case of incident P and SV waves, *Bulletin of the Seismological Society of America* 70 (1980) 1921–1941.
[28] M.A. Bravo, F.J. Sanchez-Sesma, F.J. Chavez-Garcia, Ground motion on stratified alluvial deposits for incident SH waves, *Bulletin of the Seismological Society of America* 78 (1988) 436–450.
[29] H. Kawase, Time-domain response of a semicircular canyon for incident SV, P, and Rayleigh waves calculated by the discrete wavenumber boundary element method, *Bulletin of the Seismological Society of America* 78 (1988) 1415–1437.
[30] M. Bouchon, M. Campillo, S. Gaffet, A boundary integral equation discrete wavenumber representation method to study wave propagation in multilayered media having irregular interfaces, *Geophysics* 54 (1989) 1134–1140.
[31] H. Kawase, K. Aki, A study on the response of a soft basin for incident S, P and Rayleigh waves with special reference to the long duration observed in Mexico City, *Bulletin of the Seismological Society of America* 79 (1989) 136113–136182.
[32] A.S. Papageorgiou, J. Kim, Study of the propagation and amplification of seismic waves in Caracas Valley with reference to the 29 July 1967 earthquake: SH waves, *Bulletin of the Seismological Society of America* 81 (1991) 2214–2233.
[33] B. Zhang, A.S. Papageorgiou, J.L. Tassoulas, A hybrid numerical technique, combining the finite-element and boundary-element methods, for modelling the 3D response of 2D scatters, *Bulletin of the Seismological Society of America* 88 (1998) 1036–1050.
[34] S.A. Gil-Zepeda, J.C. Montalvo-Arrieta, R. Vai, F.J. Sanchez-Sesma, A hybrid indirect boundary element-discrete wave number method applied to simulate the seismic response of stratified alluvial valleys, *Soil Dynamics and Earthquake Engineering* 23 (2003) 77–86.
[35] K.V. Nguyen, B. Gatmiri, Evaluation of seismic ground motion induced by topographic irregularity, *Soil Dynamics and Earthquake Engineering* 27 (2) (2007) 183–188.
[36] G.A. Ayala, R.A. Gomes, A general procedure for solving three dimensional elasticity problems in geomechanics, in: W. Wittke (Ed.), *Numerical Methods in Geomechanics*, A. Balkema, Rotterdam, 1979.
[37] A.H. Shah, K.C. Wong, S.K. Datta, Diffraction of plane sh waves in a half-space, *Earthquake Engineering and Structural Dynamics* 10 (1982) 519–528.
[38] D.M. Cole, P.P. Kosloff, J.B. Minster, A numerical boundary integral equation for elastodynamics I, *Bulletin of the Seismological Society of America* 68 (1988) 1331–1357.
[39] B. Gatmiri, C. Arson, K.V. Nguyen, Seismic site effects by an optimized 2D BE/FE method. I. Theory, numerical optimization and application to topographical irregularities, *Soil Dynamics and Earthquake Engineering* 28 (8) (2008) 632–645.
[40] B. Gatmiri, C. Arson, Seismic site effects by an optimized 2D BE/FE method. II. Quantification of site effects in two-dimensional sedimentary valleys, *Soil Dynamics and Earthquake Engineering* 28 (8) (2008) 646–661.
[41] K.R. Khair, S.K. Datta, A.H. Shah, Amplification of oblique incident seismic waves by cylindrical alluvial valley of arbitrary cross-sectional shape: part I. Incident P and SV waves, *Bulletin of the Seismological Society of America* 79 (1989) 610–630.
[42] K.R. Khair, S.K. Datta, A.H. Shah, Amplification of oblique incident seismic waves by cylindrical alluvial valley of arbitrary cross-sectional shape: part II. Incident SH and Rayleigh waves, *Bulletin of the Seismological Society of America* 81 (1991) 346–357.
[43] S.W. Liu, S.K. Datta, M. Bouden, A.H. Shah, Scattering of oblique incident seismic waves by a cylindrical valley in a layered half-space, *Earthquake Engineering and Structural Dynamics* 20 (1991) 859–870.
[44] T. Yokoi, F.J. Sanchez-Sesma, A hybrid calculation technique of the in direct boundary element method and the analytical solution for three-dimensional problems of topography, *Geophysical Journal International* 133 (1998) 121–139.
[45] P. Dineva, F. Vaccari, G. Panza, Hybrid modal summation — BIE method for site effect estimation of a seismic region in a laterally varying media, *Journal of Theoretical and Applied Mechanics* 33 (4) (2003) 55–88.
[46] F. Luzon, L. Ramirez, F.J. Sanchez-Sesma, A. Posadas, Propagation of SH elastic waves in deep sedimentary basins with an oblique velocity gradient, *Wave Motion* 38 (2003) 11–23.
[47] F. Luzon, V.J. Palencia, J. Morales, F.J. Sanchez-Sesma, J.M. Garcia, Evaluation of site effects in sedimentary basins, *Fisica de la Tierra* 14 (2002) 183–214 ISSN:0214-4557.
[48] R. Zhang, L. Zhang, M. Shinozuka, Seismic waves in a laterally inhomogeneous layered medium, Part I: Theory, *Transactions of the ASME* 64 (1997) 50–58.
[49] R. Zhang, L. Zhang, M. Shinozuka, Seismic waves in a laterally inhomogeneous layered medium, Part II: Analysis, *Transactions of the ASME* 64 (1997) 59–65.
[50] J. Dominguez, *Boundary Elements in Dynamics. Computational Mechanics*, Elsevier, Southampton, Amsterdam, 1993.
[51] T. Rangelov, P. Dineva, D. Gross, A hypersingular traction boundary integral equation method for stress intensity factor computation in a finite cracked, *Engineering Analysis with Boundary Elements* 27 (1) (2003) 9–21.
[52] X. Chen, A systematic and efficient method of computing normal modes for multilayered media, *Geophysical Journal International* 115 (1993) 391–409.
[53] D.G. Harkrider, Surface waves in multilayered elastic media, I. Rayleigh and Love waves from buried sources in a multilayered elastic half-space, *Bulletin of the Seismological Society of America* 54 (2) (1964) 627–679.
[54] J.E. Luco, R.J. Apsel, On the Greens functions for layered half-space, Part I, *Bulletin of the Seismological Society of America* 73 (1983) 909–929.
[55] R.J. Apsel, J.E. Luco, On the Greens functions for layered half-space, Part II, *Bulletin of the Seismological Society of America* 73 (1983) 931–951.
[56] H. Cao, V.W. Lee, Scattering and diffraction of plane P waves by circular cylindrical canyons with variable depth-to-width ratios, *International Journal of Soil Dynamics and Earthquake Engineering* 9 (3) (1990) 141–150.
[57] M. Dravinski, T.K. Mossessian, Scattering of plane harmonic P, SV, and Rayleigh waves by dipping layers of arbitrary shape, *Bulletin of the Seismological Society of America* 77 (1987) 212–235.
[58] K.L. Fishman, S. Ahmad, Seismic response for alluvial valleys subjected to SH, P and SV waves, *Soil Dynamics and Earthquake Engineering* 14 (1995) 249–258.
[59] G.F. Panza, I. Paskaleva, P. Dineva, Cr. La Mura, Earthquake site effects modeling by hybrid MS-BIEM: the case study of Sofia, Bulgaria, *Rendiconti di Scienze Fisiche by the Accademia dei Lincei* 20 (2) (2009) 91–116.
[60] C.A. Brebbia, Topics in Boundary Element Research (1987), C. Brebbia (Ed.), *Applications in Geomechanics*, Vol. 4, Springer-Verlag, 1987, p. 65.
[61] I. Paskaleva, A contribution to the seismic risk assessment of the Sofia City, Report on CNR-NATO program, 65, Announcement 219.33, 2002.
[62] K. Makra, D. Raptakis, F.J. Chavez-Garcia, K. Pitilakis, How important is the detailed knowledge of a 2d soil structure for site response evaluation? in: *12th European Conference on Earthquake Engineering*, London, 2002.
[63] E. Faccioli, M. Vanini, L. Frassine, Complex site effects in earthquake ground motion, including topography, in: *12th European Conference on Earthquake Engineering*, London, 2002.
[64] R. Paolucci, Amplification of earthquake ground motion by steep topographic irregularities, *Earthquake Engineering Structural Dynamics* 31 (2002) 1831–1853.
[65] E.H. Field, Spectral amplification in a sediment filled valley exhibiting clear basin-edge-induced waves, *Bulletin of the Seismological Society of America* 86 (1996) 991–1005.
[66] F. J Chavez-Garcia, W.R. Stephenson, M. Rodrigez, Lateral propagation effects observed at Parkway, New Zealand: a case history to compare 1d versus 2d side effects, *Bulletin of the Seismological Society of America* 89 (3) (1999) 718–732.

[67] A. Caserta, A. Rovelly, F. Marra, F. Belluci, Strong diffraction effects at the edge of the Colfiorito, central Italy, basin, in: *Second International Symposium on the Effects of Surface Geology on Seismic Motion*, Yokohama, Balkema, 1998, pp. 435–440.
[68] A. Rovelli, L. Scognamiglio, F. Marra, A. Caserta, Edge-diffracted 1-sec surface waves observed in a small-size intermountain basin (Colfiorito, central Italy), *Bulletin of the Seismological Society of America* 91 (2) (2001) 313–334.
[69] J. Miksat, Earthquake Ground Motion Modelling from Crustal and Intermediate Depth Sources, PhD Thesis, University of Karlsruhe, 2006.
[70] F. Wuttke, Inverse site identification by use of surface waves, Ph.D. Thesis, Bauhaus-University Weimar, 2005.